

**Flexible Electronics based on Inorganic Nanowires**

Journal:	<i>Chemical Society Reviews</i>
Manuscript ID:	CS-REV-03-2014-000116.R2
Article Type:	Review Article
Date Submitted by the Author:	26-Jul-2014
Complete List of Authors:	Liu, Zhe; Institute of Semiconductors, Chinese Academy of Sciences, Xu, Jing; Wuhan National Laboratory for Optoelectronics, Chen, Di; Wuhan National Laboratory for Optoelectronics, Shen, Guozhen; Institute of Semiconductors, Chinese Academy of Sciences, State Key Laboratory for Superlattices and Microstructures; University of Southern California, Department of Electrical Engineering

Cite this: DOI: 10.1039/coxx00000x

www.rsc.org/xxxxxx

ARTICLE TYPE

Flexible Electronics based on Inorganic Nanowires

Zhe Liu,^{†a} Jing Xu,^{†a} Di Chen^b and Guozhen Shen^{*a}

Received (in XXX, XXX) Xth XXXXXXXXX 20XX, Accepted Xth XXXXXXXXX 20XX

DOI: 10.1039/b000000x

Flexible electronics has gained great research interests in recent years due to their special features and potential applications in flexible displays, artificial skins, sensors, sustainable energy, etc. With unique geometry, outstanding electronic/optoelectronic properties, excellent mechanical flexibility and good transparency, inorganic nanowires (NWs) offer numerous insights and opportunities for flexible electronics. This article provides a comprehensive review of the inorganic NW based flexible electronic in the past decade, from the NWs synthesis and assembly, to several important flexible device and energy applications including transistors, sensors, display devices, memories and logic gates, as well as lithium ion batteries, supercapacitors, solar cells and generators *etc.* The integration of various flexible nanodevices into a self-powered system was also briefly discussed. Finally, several future research directions and opportunities of inorganic NW flexible and portable electronics are proposed.

1 Introduction

Over the last decades, the advancement of flexible electronics has spread across an expansive area ranging from the development of fundamental transistors, different kind of sensing devices, to flexible organic light-emitting diode displays on various kind of flexible substrates.¹⁻³ This academic interest in flexible electronics will continue for some years, driven by the growing demand for electronics with the availability of lightweight, portability, and low cost to manufacture compared to their rigid substrate counterparts, and supported by the techniques for ceaseless miniaturization of individual elements in microelectronics, for example, reductions in the critical dimensions (i.e. channel lengths and dielectric thicknesses) of transistors in integrated circuits.^{4,5} Commercially speaking, during approximately the past 15 years, the most arresting examples of macroelectronics are flat-panel displays (FPDs) which use thin film transistors (TFTs) to drive and address the active matrix pixels.⁶ While the newly commercial success of FPDs opens an era of flexible electronics, the desires for extra characteristics including light weight, low cost and portability lead to the emerge of new applications of rollable displays.⁷ Besides, thin film solar cells,^{8,9} artificial skins^{10,11} and other new applications also create intensive interests to build electronic devices directly on flexible substrates like thin plastics in scalable ways. However, the requires for flexibility and compatibility with plastic substrates which limit the process temperature to be lower than 300 °C make a great challenge to the fabrication techniques and especially the choice of materials.^{12,13}

Organic semiconductors seem to be quite suitable for these applications owing to their good flexibility, low-temperature synthesis process and inherent compatibility with plastic substrates.¹⁴⁻¹⁸ Organic electronics based on these materials have been widely investigated and applied in light-emitting diodes,¹⁹⁻²¹

radio frequency identification tags,^{22,23} sensors²⁴⁻²⁶ and so on. There still existing a problem which limits the application of organic devices, that is, the restrictions of mobility and stability. Comparing with conventional silicon based materials and organic semiconductors,²⁷⁻³² low-dimension materials with excellent electrical and optical properties have attracted intensive attention in recent years.³³⁻³⁸ Owing to their relatively higher carrier mobility and size-related intriguing physical properties, these low-dimensional materials present widely potential applications in high performance electronic devices. For example, great interest has been drawn to one-dimensional (1-D) single-walled carbon nanotube (SWCNT) based devices. With intrinsic mobility over 100,000 cm²V⁻¹s⁻¹, good mechanical flexibility and optical transparency, SWCNTs are promising candidates for high-speed electronics.³⁹⁻⁴⁸ Whereas there are still several big challenges of SWCNTs integration process such as removing metallic carbon nanotubes from semiconducting ones as well as controlling the conducting type and doping level reproducibly.^{49,50} In contrast, inorganic semiconducting NWs are ideal materials with controllable size and electrical/optoelectronic properties, and have presented one of the most interesting research directions in the nanoscience and nanotechnology.⁵¹⁻⁵³ High quality single-crystalline inorganic semiconducting NWs have been synthesized via various methods.⁵⁴⁻⁵⁶ Superior electrical properties such as high carrier mobility over amorphous silicon, amorphous oxide thin films and organic semiconductors have been found.⁵⁷⁻⁶⁰ In addition to the advantages of mobility, the problems caused by metallic carbon nanotubes also disappeared.

Besides their unique geometry structures, excellent mechanical flexibility and superior electrical properties, as inorganic NWs are capable to be transferred to all kinds of substrates, it is highly desirable to use them as the building blocks for flexible electronics in a broad and highly interdisciplinary area. First, by

providing 1-D monocrystalline pathways for carrier flow, NWs has been demonstrated to be reliable and efficient conductive channels for flexible electronics. As carriers don't have to pass through many boundaries between adjacent nanocrystals, effective mobility in flexible electronics is largely improved. Second, for its high specific surface, inorganic NWs has also been demonstrated to act as highly sensitive materials for flexible electronics, especially for the sensing devices. Third, inorganic NWs own excellent mechanical flexibility which mainly comes from three aspects: 1) With the materials' dimensions reducing to nanometer scale, mechanical strength of inorganic NWs is usually far superior to their bulk counterparts because of a reduction of defect incorporation. This characteristic is very common and indeed expected in many nanoscale materials. For example, average Young's modulus of ZnO NWs is very close to that reported for its bulk and thin-film values while the ultimate strengths are up to 40 times that of their bulk counterpart.⁶¹ 2) It is well known that propensity for crack formation in semiconductor materials is linearly reduced with dimensions.⁶² In other words, inorganic NWs can be more reliable and robust under bending conditions when compared with their bulk one. 3) Inorganic NWs itself only cross over a span of micrometer scale and often serve as some vital but tiny parts of an electronic device or a system. This feature allows inorganic NWs to avoid the macroscopic deformations caused by the structural damage in the bulk materials cases.

To fulfil fully flexible electronics, flexible, lightweight, and miniaturized energy conversion/storage devices are recognized as one of the key components. However, the conventional energy conversion/storage devices are too bulky and inflexible to integrate with the above flexible electrical/optoelectronic devices even on the common forms of flexible substrates. The lack of flexible energy conversion/storage unites gives a natural limit on the further development of next-generation flexible devices, and as a result, several enabling technologies must be developed to realize flexible energy conversion/storage devices with optimized performance. Very recently, several simple but inspirational models have been demonstrated including supercapacitors and lithium ion batteries. Flexible photovoltaic has also being considered as the harvesting of energy from sunlight and conversion into electrical power.^{63,64}

This article reviews the state-of-art research progress in the field of flexible electronics based on inorganic NW materials. It begins with the preparation and assembly techniques of basic materials in section 2 and concentrate on the various applications from section 3 to section 5 including basic flexible electronic device elements like transistors, sensors, displays, memories, logic gates, etc. Since flexible energy conversion/storage devices are vital to realize fully flexible electronic/optoelectronic systems, to this point, a number of recent developed flexible energy conversion/storage devices were discussed and summarized in the following sections. Finally, we will discuss the future challenges and perspectives of inorganic NWs based flexible electronics.

2 Inorganic NW synthesis and assembly

2.1 NW synthesis

Inorganic NWs can be prepared through a variety of methods,

among which bottom-up approach is a summary of various routes using basic elements to synthesize NW materials.^{65,66} Numerous kinds of materials such as metals, inorganic compounds and polymers are prepared by bottom-up approach successfully.⁶⁷⁻⁶⁹ In general, preparation of 1-D nanomaterials relies on the ability to condense and grow an assembly of atoms by breaking the symmetry of their crystal lattices which can be realized through controlling the surface energies of different crystal faces, templates assisted growing or catalyzed synthesis. Synthesis of NWs has been well-documented in the last several years, thus they are not the focus of this review and we only provide a very brief introduction about NWs synthesis in this section.

The first strategies that have been widely applied are solution-based methods including hydrothermal method, solvothermal method, reflux method, microwave synthesis method and so on.⁷⁰⁻⁷² At the beginning of the synthesis, nucleation results in the formation of massive nanocrystals with different crystal faces exposed to the solution. The diversity of surface energies will lead to anisotropic condensation or growth of these nanocrystals. If one of the crystal faces has a distinct surface energy, a preferred growth on this face will result in the formation of one dimensional morphology.⁷³ What is worth noting is that the surface energies are not only the intrinsic properties of materials, but also affected by the solution environment or the choice of source reagents. PH values of the solution are often investigated to control the growth of NWs, while some specific cations or anions are also observed to play important roles in the formation of 1-D structures. For example, Xu *et al.* studied the effect of capping agent, metal cations as well as pH values on hydrothermal growth of 1-D ZnO nanostructures.⁷⁴ It was found that long chains of oleate ions led to the formation of ZnO NWs (Fig.1a) and nanorods, compared to CH_3COO^- or Cl^- . Similar phenomena were also found in Birkel's result.⁷⁵

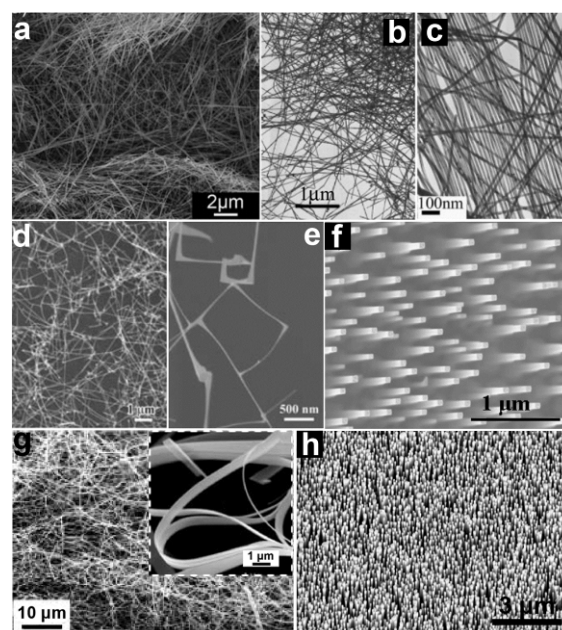


Fig. 1 SEM images and TEM images of various types of 1-D nanostructures grown from both solution process and vapor phase processes. (a) ZnO NWs obtained via hydrothermal method. Reprinted with permission from ref. 74 © 2011, The Royal Society of Chemistry.

(b-c) Ag nanocables via hydrothermal method. Reprinted with permission from ref. 76 © 2005, WILEY-VCH. (d-e) In_2O_3 NW thin films via VLS method. Reprinted with permission from ref. 79 © 2010, WILEY-VCH. (f) ITO NW arrays via an epitaxial growth method. Reprinted with permission from ref. 92 © 2006, WILEY-VCH. (g) SnO_2 nanobelts via VS method. Reprinted with permission from ref. 100 © 2003, American Institute of Physics. (h) well-aligned ZnO NWs via the VS method. Reprinted with permission from ref. 103 © 2005, American Institute of Physics.

Solution phase methods have been extensively explored to synthesize various NWs. Metallic NWs like Ag (Fig.1b-c), Cu, Au, and Pt,^{76,77} semiconducting oxide NWs such as ZnO, SnO_2 , In_2O_3 , Cu_2O , Fe_2O_3 and V_2O_5 have been successfully synthesized.⁷⁸ In spite of the decreased crystallinity and weakened electrical properties, it can be predicted that solution phase methods are promising ways for mass production and large scale application of NWs with the advantages of low cost and easy fabrication.

Large aspect ratio often helps to enhance the contact of the electrodes with the active materials in electronic devices like transistors.⁷⁹ It also facilitates the adsorption/desorption of O_2 in optoelectronic devices such as photodetectors.⁸⁰ That is why NWs find such a wide application in nano-devices. However, it is usually a challenge to synthesize uniform NWs, especially highly ordered NW arrays, by using general hydro/solvothermal methods. In this case, templates are adopted to control the material's growth in a confined domain or along a specific direction. Among all adopted templates anodic aluminium oxide (AAO) membrane are widely utilized. As a typical example, highly ordered CdS NWs array with lengths up to 1 μm and diameters as small as 9 nm have been obtained by using AAO templates. During the process, CdS was electrochemically deposited into the pores of AAO films from an electrolyte containing Cd^{2+} and S in dimethyl sulfoxide and the deposited material was found to be hexagonal CdS with the crystallographic c-axis preferentially oriented along the length of the pore.⁸¹ Similar method were also employed to synthesize many other 1-D nanostructures, such as In_2O_3 , SnO_2 , Fe_2O_3 and Fe_3O_4 NWs.^{79, 80-84}

For the vapor phase processes, an important one is using catalysts to guide the growth of NWs which is generally described as vapor-liquid-solid (VLS) method.⁸⁵ In VLS growth process, metal droplets, usually formed by annealing a gold thin film prepared by sputtering (1-10 nm) or gold colloids,⁸⁶ are indispensable to serve as catalysts. These metal droplets capture the source vapor and form liquid alloy droplets, then supersaturation and nucleation happen at the liquid/solid interface and lead to axial crystal growth. Owing to catalyzed mechanism, the NWs often have diameters equal to the droplets, and only grow at sites activated by metal droplets. VLS method was first developed by Wagner and Ellis to synthesize single crystal Si NWs and became one of the most successful approaches for preparation of various kinds of NWs,⁸⁷ including element semiconductors like Si and Ge, metal oxides like ZnO and In_2O_3 (Fig.1d-e), II-VI group semiconductors like ZnS and CdSe, III-V group materials like GaAs and InP, and others.⁸⁸⁻⁹¹

Using appropriate substrate, well-aligned NW arrays can be fabricated with the orientation normally perpendicular to the substrate surface through catalyzed epitaxial growth. For

example, vertical aligned tin-doped indium oxide (ITO) NW array has been synthesized using ITO thin film as substrate, as shown in Fig.1f.^{92, 93} Besides the ability to tune the diameters of NWs by changing the catalysts' sizes, one of the advantages of VLS method is the possibility to control the orientation, position and density of NW arrays which are very important to the assembly of NWs for device applications, through patterning the catalyst nanoparticles. Combining the epitaxial growth technique and nano-scale patterned metal catalysts fabricated by electron-beam lithography, photolithography, mask lithography by porous alumina or nanosphere lithography, highly ordered vertical aligned ZnO NW arrays with different densities have been successfully synthesized in hexagonal, orthogonal or other kinds of arrangements.^{94, 95}

In addition, different kinds of heterostructures along axial or radial directions are also available through clever synthesis strategies. Branched NWs can be fabricated using two-step VLS growth method, which has been utilized for SnO_2 hierarchical NWs.⁹⁶ Besides, NWs can be formed with different materials in core-shell layout by controlling growth conditions to induce homogeneous reactant decomposition on the core NW surface.⁹⁷ Through repeated modulation of reactants, even multishells can be obtained. Axial heterostructures have also been formed by a time-dependent modulation of NW composition and doping during the growing process. These heterostructured NWs are essential for many potential applications in nanoscale optoelectronic devices.

Another process related to VLS method that has also been employed in the growth of NWs is named vapor-solid (VS) technique. The VS technique does not require metal droplets serving as catalysts. But meanwhile, a higher temperature is usually needed to overcome the much higher activation energy compared with VLS method.⁶³ Metal oxide NWs such as ZnO,⁹⁸ SnO_2 (Fig.1g),⁹⁹ In_2O_3 ,¹⁰⁰ CdO¹⁰¹ and many other NWs have been successively synthesized via the VS process in recent years, demonstrating its universality towards various NWs. In catalysts-assistant growth, the remains of catalysts or additives will unavoidably influence the purity of the final products, thus the fundamental properties of the materials will inevitably be affected. NWs synthesized via VS process may also have high crystallinity and outstanding microstructure. For example, Zhang *et al.* have reported a simple vapor solid deposition approach to synthesize well-aligned ZnO NWs on c-oriented ZnO thin films using Zn as vapor source.¹⁰² As shown in Fig.1h, well-aligned NWs are in high density and are uniformly distributed over the substrate.

2.2 NW assembly and device fabrication

Between NW synthesis and device fabrication, a key challenge is the controlled assembly of NWs. In the initial phase of NW device, researches are concentrated on individual devices. NWs are directly suspended in solutions and dropped onto substrates. Randomly distributed and arranged NWs are obtained after volatilize the solutions. These individual devices are fabricated to investigate the electrical transport properties of NWs. However large scale device arrays and integrated circuits are impossible based on this method due to the disordered arrangement of NWs. In order to overcome this challenge and tap the potential of NWs in flexible electronics, several post-growth techniques are

developed. NWs assembly is not the focus of this review and Javey in UC Berkeley and Fan in HKUST have already provided very good reviews focusing on NWs assembly, thus we only give some brief introduction on NWs assembly here.

One of the earliest approaches to assemble NWs is the fluidic alignment in microchannels. Huang et al. construct fluidic channels on flat substrates using poly (dimethylsiloxane) (PDMS) mold.¹⁰³ NW arrays are then assembled by passing suspensions of NWs through these channels. Fig. 2a shows the SEM image of InP NWs assembled on flat substrate, showing that NWs are aligned along the flow direction. By controlling the flow rate, more than 80% of the NWs can be aligned within $\pm 5^\circ$ of the flow direction. Combined with surface-patterning methods to modify the surface chemical functionality, fluid flow can generate well-ordered NW parallel arrays. With the use of layer-by-layer scheme, this approach can also be used to organize NWs into more complex crossed structures which are critical for building dense electronic device array.

NWs can also be organized within blown-bubble films. The shear stress created by expanding the NW suspension bubble is utilized by Yu et al to align the high aspect ratio NWs along the principle direction of strain, as shown in Fig. 2b.¹⁰⁴ In this approach, a homogeneous polymer suspension of NWs is first prepared and then expanded using a circular die to form a bubble at controlled pressure and expansion rate. The shear force formed during the expansion leads to alignment of NWs. The aligned NW density can also be controlled by the concentration of suspensions. The organized NW blown-bubble film can be transferred to flexible plastic sheets as well as highly curved surfaces, showing great potential for large area flexible electronic application.

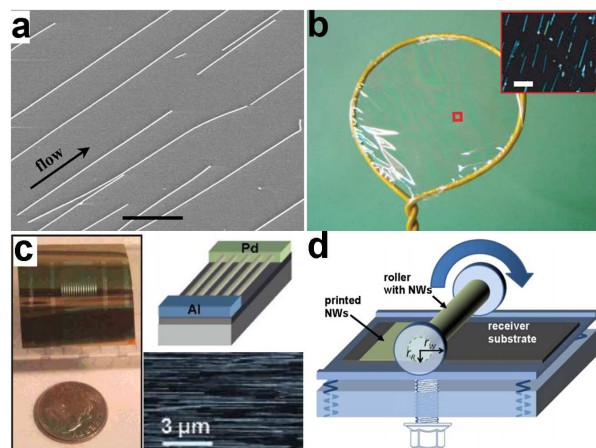


Fig. 2 (a) SEM images of parallel arrays of InP NWs aligned by channel flow. Reprinted with permission from ref. 103 © 2001, American Association for the Advancement of Science. (b) Illustration of the blown bubble film NW alignment. Inset is the dark-field optical image showing Si NWs in the film. Reprinted with permission from ref. 104 © 2007, Macmillan Publisher Ltd. (c) Optical image of a novel diode structure fabricated on parallel arrays of p-Si NWs assembled by contact printing method. The upper right is the schematic of the Pd-Al contacts and the lower right is the regular array assembly of single Si NWs. Reprinted with permission from ref. 107 © 2008, American Chemical Society. (d) Schematic of the differential roll printing setup. Reprinted with permission from ref. 109 © 2007 American Institute of Physics.

Other methods to assemble NWs include the Langmuir-

Blodgett (LB) technique and field-assisted orientation. LB technique is widely used to deposit organic monolayers from a liquid surface to a solid substrate. In order to form NW monolayers, NWs are first functionalized with surfactant and dispersed on the water surface. When the NWs are compressed, they will organize as parallel arrays with their longitudinal axes perpendicular to the compression direction. Electric and magnetic fields are also utilized by Smith and Hangarter to assemble NWs.¹⁰⁵ However, their methods are limited to metallic or magnetic NWs. In another way, Freer et al. use dielectrophoretic approach to achieve a 98.5% yield of single NWs assembled over 16,000 patterned electrode sites with submicrometer alignment precision. By carefully controlling the hydrodynamic and dielectrophoretic forces, single NWs can be assembled on each pair of electrodes with high probability.¹⁰⁶

Recently, a new NW assembly approach called contact printing draws much attention with the advantages of high efficiency, large scale and the compatibility with printing electronics. As shown in lower right of Fig. 2c, the alignment of NWs is realized by directionally sliding the grown substrate with a dense “lawn” of NWs on top of the receiver substrate coated with patterned photoresist. During the process, NWs are anchored on the receiver substrate by contacting and aligned by the sliding step. Multilayer NWs are assembled by Javey et al. using this approach and are used as building blocks for three-dimensional, multifunctional electronic devices.¹⁰⁷ Fan et al. improve this dry transfer method by introducing a lubricant during the transfer process, which serves as a spacing layer between two substrates and minimizes the friction between NWs.¹⁰⁸ As a result, the uncontrolled breakage and detachment of NWs are prevented and highly ordered NW arrays are obtained. The printed NW density can also be modulated by appropriate surface chemical modification. Both dense and single NW arrays can be aligned through pre-patterning the receiver substrates. To further extend this approach for scalable and large area application, a differential roll printing (DRP) process is developed. As shown in Fig. 2d, an important aspect of this strategy, as compared to previous methods, is the use of cylindrical grown substrate.¹⁰⁹ NWs are deposited using VLS process on glass or quartz tubes. The grown tube is then used as the roller and brought into contact with the pre-patterned receiver substrate. By rolling the tube with a controlled velocity, NWs are detached and transferred to the receiver substrate. This process provides a new approach for NW transfer and assembly in a cost-effective and large area manner.

Electrospinning is an efficient technology to fabricate randomly oriented and coiled NWs on certain substrates. Modified electrospinning method was introduced to print large-area organic semiconductor NW arrays uniformly with desired orientation and position.¹¹⁰⁻¹¹² This kind of method has many outstanding advantages: 1) It fits for different types of NWs, such as organic NWs arrays with poly (3-hexylthiophene) (P3HT) and poly (ethylene oxide) (PEO) as the precursors, etc. 2) Semiconductor NW arrays can be successfully printed on almost any kind of substrate, such as SiO₂/Si, flexible polyarylate (PAR) or even common paper. 3) High-speed and large-area printing is another attractive advantage of this method. 4) The diameter of the NWs, the distance between NWs, and the NW density can be precisely controlled. All these advantages guarantee highly

significant device fabrication work on the following steps and a piece of typical work based on this method will be fully discussed in the following transistor section.

The successful synthesis of NWs and printing of NWs arrays makes it possible to fabricate flexible electronic devices. The fabrication process for flexible electronic devices is similar to that of rigid electronic ones, that is, photolithography process followed by micro/nano-electrode metallization and lift-off. First, traditional photolithography is used to pattern contact areas onto the both ends of the NW or NW arrays. Specifically, after NWs growth and assembly on the flexible substrate, the photoresist (positive or negative) is spin coated onto the substrate followed by exposure using UV lithography machine with a patterned photolithography mask. The photoresist over unwanted areas is then removed using developing solution. Then, the metal film is evaporated over the surface and the remaining photoresist is removed using acetone. At last, the electrodes over the contact areas are annealed at a proper temperature in an inert atmosphere to enhance the contact between the NWs and the electrodes. This photolithography, metallization and lift-off processes have shown themselves to be very resourceful at fabrication of various flexible electronic devices before. For example, by adjusting the electrode materials, symmetric or asymmetric contact between the NWs and the electrodes can be obtained. Fig. 2c shows a Schottky diode with asymmetric PA-Al contacts at different ends of the NWs, that is, the Pd forming a near Ohmic contact to the valence band and Al resulting in a Schottky interface. Besides, by adopting different modes of electrodes (T-shaped gate, top-gate, Ω -gate *et al.*), by changing different dielectric films, by improving the surface passivation quality, or even via e-beam lithography techniques, more sophisticated flexible device at smaller sizes can be fabricated.

3 Inorganic NWs based flexible electronic devices

Since organic materials can be formed into NWs with excellent flexibility, it is necessary to give a brief introduction on flexible electronics based on organic NWs, with a focus on their advantages as well as disadvantages. Recent reports demonstrated that organic materials in 1-D structure forms ranging from nanotubes to NWs can be really used for various applications in flexible electronics.¹¹³⁻¹¹⁷ These 1-D structures can be grown or fabricated by both bottom-up or top down strategies. For example, Fig. 3a gives a detailed description of the home-built printer used to print organic NWs.¹¹⁰ In this electrospinning process, organic precursors were injected through a metal nozzle at a predefined rate. An x-y stage driven by a high-speed motor served as the collector. When applying a high voltage between the nozzle tip and the collector and moving the target substrate at a certain direction at the same time, organic NWs can be well aligned on the receive substrates with a desired orientation, as shown in the inset. Fig. 3b shows the large-area organic NW based transistors array on flexible PAR substrate, potentially offering the performance that required for new type of electronics along with desired transparency and flexible characteristics. Fig. 3c shows the large-area uniform copper phthalocyanine (CuPc) NWs with proper density and a high degree of orientation on the polyurethane acrylate (PUA) grating substrate, which was an ideal candidate for flexible optoelectronic devices.¹¹⁶

Organic NWs offers the possibility of direct NWs printing and NW-based flexible devices' integration. Organic NWs have the following advantages. 1) Organic NWs can be synthesized from simple, cost-effective, and scalable processes, which have shown promise for their assembly into functional systems. 2) Physical parameters of organic NWs such as size, orientation, surface states, defects and polarization *et al.* can be easily controlled. 3) The relatively high degree of transparency has been proved to be very important for designing next-generation flexible electronic devices. For example, "see-through" electronic displays, as one kind of whole new conceptual product, has attracted a lot of attention in recent years. On the other hand, organic NWs still have some drawbacks. 1) The relatively low mobility of organic NWs often leads to poor performance of the final devices, thereby restricting the range of application possibilities. 2) High contact resistance as well as mismatched interfaces between organic NWs and the metal electrodes also lead to a further worsening of final device's performance. 3) Organic NWs doesn't enjoy full compatibility with existing IC manufacturing process for its poor heat tolerance. 4) If organic NWs are introduced to the large-scale commercial production, the organic pollution is an obvious feature, and sometimes unavoidable.

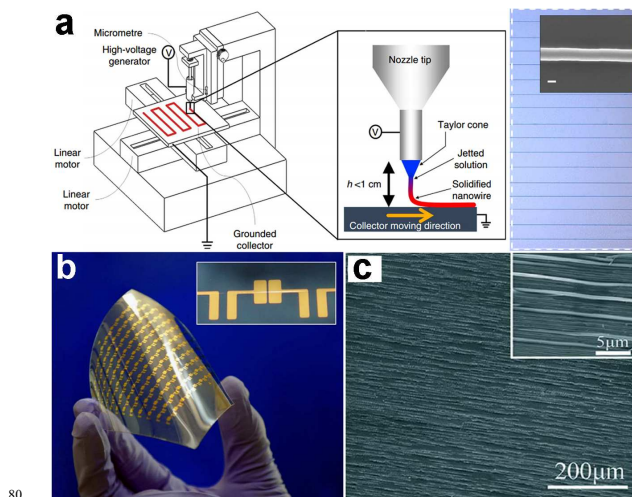


Fig. 3. (a) Schematic diagram of organic semiconductor NW printing and inset is the optical image of the well aligned organic NWs. (b) Large-area organic NWs FET array on flexible PAR substrate. Reprinted with permission from ref. 110 © 2013, Macmillan Publisher Ltd. (c) SEM image of organic CuPc NW arrays. Reprinted with permission from ref. 116 © 2012, The Royal Society of Chemistry.

As we mentioned in the introduction part that inorganic NWs have several superior features compared with organic NWs, thus in the following parts, we will give details on flexible electronics based on inorganic NWs, ranging from basic electronic devices such as transistors to sensors, photodetectors and other complicated devices.

3.1 Electrodes

The development of flexible electronics requires high quality electrodes with a combination of high electrical conductivity and high flexibility, as well as optical transparency. Indium tin oxide (ITO) is the commonest choice for most current flexible nanodevices because of its high transmittance and conductivity. However, considering the scarcity of the indium and brittlement

of the ITO film, a new class of conducting material which can replace the ITO film should be designed. Recently uniform conducting films such as carbon nanotube films, graphene films and especially metal NW films have been considered as stretchable and foldable conductors. For example, Madaria *et al.*¹¹⁸ fabricated Ag NWs electrode using a dry transfer printing technique on flexible polyethylene terephthalate (PET) substrates. The obtained conducting films show strong adhesion to a PET substrate over a large area with a low sheet resistance of 10 Ω /sq and a transparency of 85%, comparable to the conventional ITO films. Such a process also allows the preparation of high quality patterned films of silver NWs with different line widths and shapes, allowing the possible application of flexible electronic circuits. Details about the preparation of Ag conducting film were illustrated in Fig. 4a-c. Another example is the use of a Meyer rod coating method for the fabrication of Ag NWs based transparent electrodes.¹¹⁹ Ag NWs ink in methanol solution with a concentration of 2.7 mg/mL was prepared as the coating agent. As shown in Fig. 4d-f, pre-sonicated Ag NWs ink is dropped onto a PET substrate. Then, a Meyer rod is either pulled or rolled over the solution, leaving a uniform, thin layer of NWs network. After drying the film at a proper temperature, Ag NWs based electrodes with specular transmittance of \sim 80% and with sheet resistance of 20 Ω /sq can be achieved. Such method is also applicable for other transparent metal NWs electrodes, such as copper,¹²⁰ a metal with the electrical resistivity almost as good as that with silver.

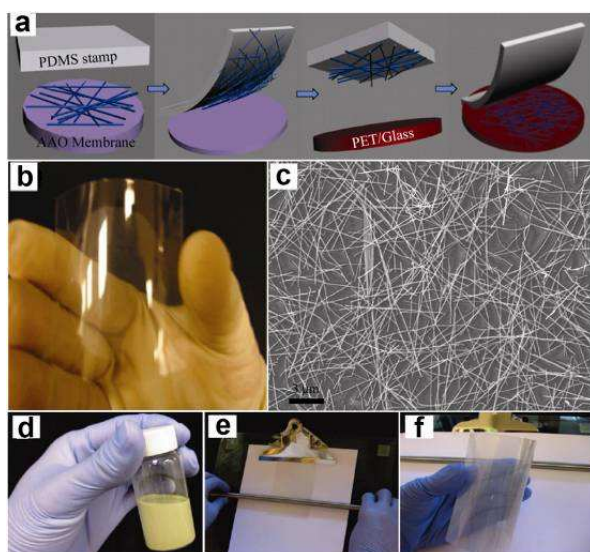


Fig. 4. (a) Schematic illustration of the transfer process of Ag NW networks from growing AAO substrate to the PET or glass substrate. (b-c) Photograph of a NW film on PET substrate and SEM image of the network, respectively. Reprinted with permission from ref. 118 © 2010, © Springer. (d-f) Schematic illustration of Meyer rod assisted coating method for Ag electrodes. Reprinted with permission from ref. 119 © 2010, American Chemical Society.

3.2 Transistors

Field-effect transistor (FET) is the most important and basic component in electronics. NWs are widely investigated, recently as the building blocks for flexible FETs, such as silicon, metal oxides and other compound semiconductors. To meet the demand for high speed devices, inorganic semiconductor NWs with high mobility are desired. Flexible InAs NW array FETs working on

radio frequency were demonstrated by Takahashi *et al.* (Fig. 5a-b).¹²¹ The high-frequency performance of the InAs NW array FETs were analyzed by measuring two-port scattering parameters (S parameters) in the common-source configuration over a frequency range from 40 MHz to 10 GHz. Derived from these S parameters, The current gain (h_{21}), maximum stable gain (MSG), and unilateral power gain (U) extracted from the measured S parameters as a function of frequency are shown in Fig. 5c. The InAs NW FETs exhibit an impressive maximum frequency of $f_{\max} = 1.8$ GHz and a cutoff frequency $f_t = 1.08$ GHz. At 1 GHz, the MSG reaches \sim 6 dB, indicating that designing an RF amplifier at GHz region is plausible based on InAs NW FETs. The high-frequency response of the devices is due to the high saturation velocity of electrons in high-mobility InAs NWs. More importantly, the InAs NW FETs do not exhibit significant electrical degradation even when bent to a radius of \sim 18 mm, showing excellent mechanical flexibility. The unique characteristics in terms of large on-current (I_{on}), large transconductance (g_m), high mobility and impressive maximum frequency from the InAs FETs pave an avenue to develop the next-generation high-performance semiconducting elementary unit for multifunctional optoelectronic device applications in the future.

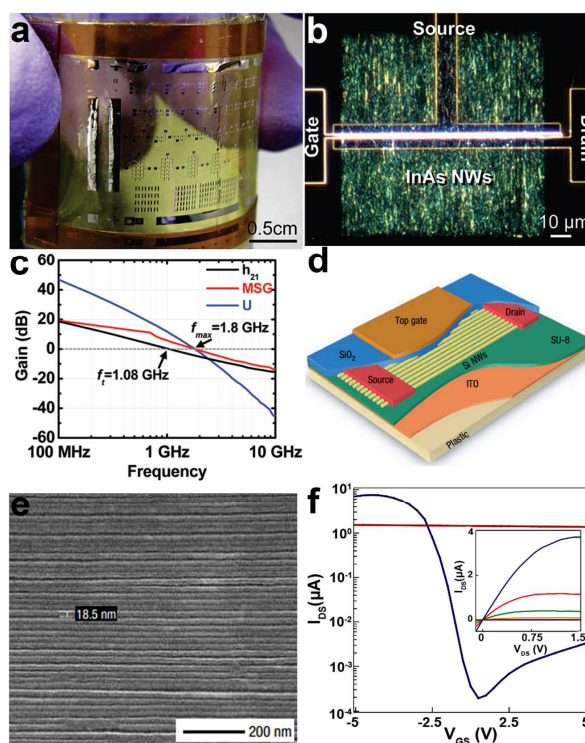


Fig. 5 Optical image of (a) the printed InAs NW array FET fabricated on a flexible PI substrate and (b) the InAs NW region. (c) High-frequency behaviour of the InAs NW array FET. Reprinted with permission from ref. 121 © 2010, American Chemical Society. (d) Schematic illustration of the p-type Si NWs array based TFT and (e) is the SEM image of the aligned NWs. (f) I_{DS} versus V_{GS} ($V_{\text{DS}}=1$ V) for a p-type Si NWs array based TFT. Inset is the I_{DS} versus V_{DS} curves correspond to $V_{\text{GS}}=-5, -4, -3, -2, -1$ and 0 V, respectively. Reprinted with permission from ref. 122 © 2007, Macmillan Publisher Ltd.

In order to build power-efficient flexible logic gates and integrated devices, both n-type and p-type semiconductor NWs

are required. However, most of the currently investigated NWs are n-type semiconductors. Flexible p-type NWs FETs are rarely reported. Doping is the first-thought routine to modify the conducting type of the NWs that used in flexible FETs, from n-type to p-type. Mcalpine *et al.* present a scalable and parallel process for transferring hundreds of pre-aligned p-type silicon NWs onto plastic to yield highly ordered films for flexible FETs.¹²² Fig. 5d shows the schematic illustration of the flexible FETs with the electrodes and various labeled layers. Plastic served as the bendable substrate and 2- μm -thick SU-8 epoxy was used as a gate dielectric in this device. Fig. 5f shows the electronic performance of the top-gate FETs containing about 200 p-type Si NWs. Inset of Fig. 5f shows I_{ds} - V_{ds} curves at different V_{gs} from 0 V to -5 V, with negatively increasing gate voltage, the conductance of the device was gradually suppressed, demonstrating the p-type nature of the B-doped Si NWs.

Another interesting work on flexible p-type FETs are PbSe NWs FETs encapsulated in polymethyl methacrylate (PMMA).¹²³ PbSe NWs were aligned under an electric field on varying dielectric stacks and fabricated into flexible FETs operated on kapton films, and aluminum oxide (30 nm) was used as the back gate dielectric and octadecylphosphonic acid (ODPA) was used to passivate the aligned NWs. The obtained device exhibited ambipolar characteristics, as evidenced by the electron transport in the I_{ds} - V_{gs} curves. Predominantly p-type nature under negative bias voltage was observed, and moreover, predominantly n-type nature for positive gating was also confirmed the ambipolar characteristics of this PbSe device. Contrary to the colloidal PbSe NW (NW) and nanocrystal (NC) FETs, this PMMA encapsulated PbSe NW arrays showed quite low-hysteresis (< 1V).¹²⁴

3.3 Sensors

With controllable geometry and high surface areas, NWs exhibited excellent response to outer environments, such as optical radiation, temperature variation, pressure differential, chemical molecules, pH value, proteins and DNA *et al.*¹²⁵ In this section, we highlight several recent significant results that have made impacts toward the field of flexible and stretchable sensors, including photodetectors, stress sensors and artificial skins.

3.3.1 Photodetectors

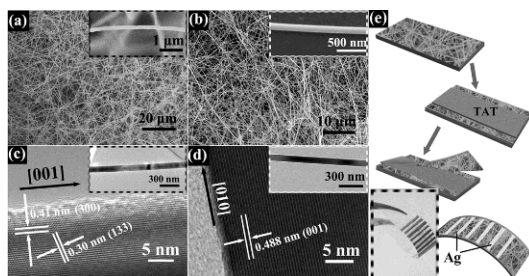


Fig. 6 SEM images of (a) Zn₂GeO₄ and (b) In₂Ge₂O₇ NW networks prepared for flexible photodetectors. (c-d) TEM images of these two as-synthesized NWs, respectively. (e) NW networks transfer and flexible device fabrication process for a representative photodetector based on PET substrate. Reprinted with permission from ref. 38 © 2012 Optical Society of America.

Photodetector is one of the most important applications of semiconductor NWs and has attracted extensive attentions recently. Photoresponse of NWs to light irradiation with different

wavelengths mainly depends on their band gap. For instance, with large band-gaps, metal oxide NWs such as ZnO,¹²⁶ SnO₂¹²⁷ and In₂O₃¹²⁸ NWs are widely studied for the fabrication of high performance ultraviolet (UV) photodetectors. Metal chalcogenides NWs with moderate band gaps such as ZnSe,¹²⁹ Sb₂Se₃¹³⁰ and In₂Se₃¹³¹ are chosen as the active materials for visible light photodetectors. Narrow band-gap semiconductors such as In₂Te₃¹³² and InAsSb¹³³ NWs have been demonstrated as sensitive materials for infrared photodetectors. In this section, the latest developments of flexible NW photodetectors are summarized, focusing on three types of photodetectors: NW networks based photodetectors, individual NW based photodetectors and NW arrays based photodetectors.

NW networks, or NW thin films, are emerging as promising structures for photodetectors as its advantage in easy device fabrication process. High performance photodetectors can be fabricated on various NWs thin films such as ZnO, SnO₂, In₂O₃, and multicomponent metal oxides. For example, Yan *et al.* synthesized Zn₂GeO₄ NW networks and fabricated efficient ultraviolet photodetectors on SiO₂/Si substrate by using photolithography technique.^{134,135} However, expensive and tedious photolithography techniques were required in Yan's work, which would certainly hurdle the practical application of NW networks based photodetectors. Recently, flexible photodetectors were fabricated on Zn₂GeO₄ and In₂Ge₂O₇ NW networks as shown in Fig. 6. High quality single crystalline Zn₂GeO₄ and In₂Ge₂O₇ NW networks were synthesized via a conventional CVD method. By simply transferring the NW mats to a transparent adhesive PET tape and printing the silver paste parallel lines which served as the electrodes, flexible photodetectors were successfully fabricated. Both Zn₂GeO₄ and In₂Ge₂O₇ NW networks based flexible photodetectors exhibited excellent photoconductive performance in terms of high sensitivity, excellent stability, and fast response and recovery time to the UV light.

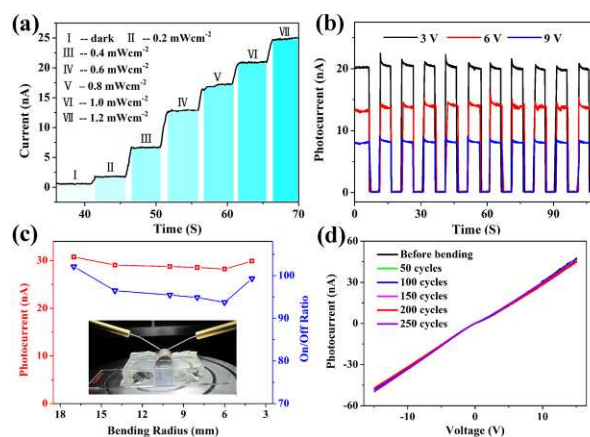


Fig. 7 (a) Photoresponse of the flexible ZnTe NWs photodetector under an improved incident light level and (b) at different bias under the same illumination (532nm, 1.2mW/cm²). (c) The magnitude of photocurrents (red) and the corresponding on/off ratio (blue) under different bending radii. Inset is the optical micrograph of the experimental setup. (d) I-V curves measured before and after different bending cycles. The operation voltage of Figs. 5 (a) and 6(c) are 12.5 V and 9 V, respectively. The light intensity of (c, d) is 1.4 mW/cm². Reprinted with permission from ref. 56 © 2013 Optical Society of America.

Single NW based photodetectors are the most common NW based optoelectronic devices. It can be easily fabricated via UV photolithography or e-beam lithography techniques followed with metal film deposition techniques. Single NW photodetector is thought to be the most effectual one that could directly and quantitatively study the light acquisition as well as the optical-to-electrical conversion process. As an example, single ZnTe NW based flexible photodetectors were recently reported.⁵⁶ ZnTe NWs (Fig. 7a) was shown to be p-type conductivity with an effect mobility of $11.3 \text{ cm}^2/\text{Vs}$ and the corresponding flexible photodetectors were proved to have the features of excellent flexibility, stability and sensitivity to visible incident light. As shown in Fig. 7b, the flexible device has a very stable photocurrent-switching behavior under different light irradiance conditions, indicating its sensitivity to the very slight variations in incident light. In Fig. 7c, the device was bent to different curvature radius to precisely assess the optoelectronic performance of the device. The photocurrents maintained at about $30 \pm 1.2 \text{ nA}$ and the on/off ratio stayed at the level of 98 ± 4 under the certain test condition. Besides, Fig. 7d showed the I-V curves of the flexible ZnTe photodetectors after 50, 100, 150, 200 and 258 cycles of bending, no obvious current degradation was recorded, indicating the mechanical robustness and electronic stability of the flexible device.

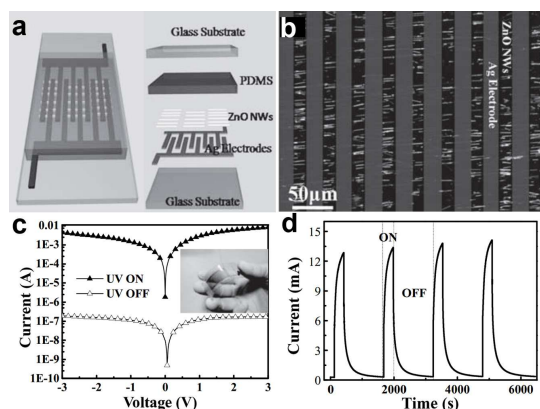


Fig. 8 (a) Schematic design of an integrated UV sensor. (b) Optical image of ZnO NWs connected in parallel between Ag electrodes. (c-d) I-V curves and time-dependent photoresponse of the flexible UV sensor with/without UV illumination, respectively. Inset of (c) is the optical image of a flexible integrated NW UV sensor. Reprinted with permission from ref. 136 © 2011, WILEY-VCH.

Ordered NW array is a simple and efficient remedy for low-level photocurrent faced in single NW based photodetectors. Many technical methods have been summarized above to design arranged NWs, and the obtained NW arrays could be transferred to the flexible substrate directly for the fabrication of flexible nanodevices. In the report of Bai *et al.*, integrated ZnO NW UV photodetectors were fabricated on rigid glass and flexible PET substrates at the macroscopic scale.¹³⁶ As shown in Fig. 8a-b, cross-finger shaped Ag electrodes were pressed onto the aligned ZnO NWs and provided an Ohmic contact between the Ag electrodes and the ZnO NWs on the PET substrate, which is confirmed by the I-V measurements in Fig. 8c. We can find that the photocurrent is about five orders of magnitude larger than the dark current, giving a very large ON/OFF ratio. Time-resolved UV photoresponse measurements under UV irradiance of 4.5

mW cm^{-2} and 3 V bias was shown in Fig. 8d, confirming the ultrahigh ON/OFF ratio. This ultrahigh ON/OFF ratio implies the ability to sense weak UV incident light even in the high noise level environment. Using contact printed aligned NW arrays (Zn_3As_2 , Zn_3P_2 , etc.) as the active materials, different types of high performance flexible photodetectors were also successfully fabricated, with typical response to light irradiation with different wavelengths.¹³⁷ In fact, flexible NWs array based photodetectors are promising building blocks for next generation stretchable optoelectronic devices. Undoubtedly, more research results and exciting discoveries lie ahead.

3.3.2 Stress sensors

Stress sensing or pressure sensing is another important sensing property of NWs. Experiments have demonstrated the potential of NWs as stress sensors. For example, in Yang's work, piezoresistance effect of silicon NWs instead of Si bulk that can be applied to stress sensors was systematically studied.¹³⁸ To be specific, individual p-type Si NW with $\langle 111 \rangle$ or $\langle 110 \rangle$ growth directions were grown in trenches on silicon-on-insulator (SOI) wafers to form bridge structures. Then quantitative relation between conductivity and stress/strain was measured by the four-point bending method and corresponding piezoresistance coefficient along the growth direction was calculated. It was found that the conductance increases under compression and decreases under tension for a p-type $\langle 111 \rangle$ oriented Si NWs. Enhanced longitudinal piezoresistance coefficients as high as $-3550 \times 10^{-11} \text{ Pa}^{-1}$ was obtained, in comparison with a bulk value of $-94 \times 10^{-11} \text{ Pa}^{-1}$. This giant piezoresistance effect in Si NWs may lead to good application prospect of NW-based flexible stress sensors.

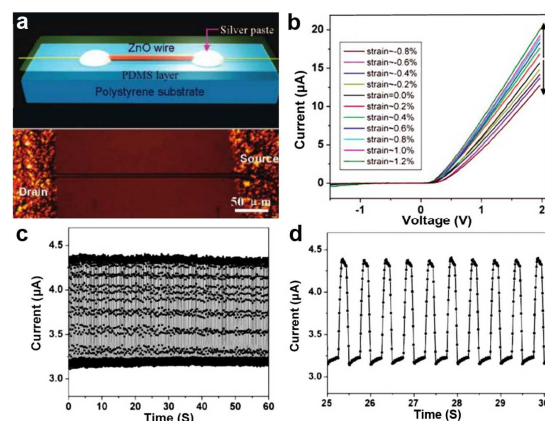


Fig. 9 (a) Schematic (up) and optical image (bottom) of the flexible single ZnO based strain sensor device. (b) Typical I-V curves of the sensor at different strained conditions. (c-d) Current response of the flexible stress device that was repeatedly stretched at a frequency of 2 Hz under fixed bias of 2V. Reprinted with permission from ref. 139 © 2008, American Chemical Society.

Technically, the Si-NW bridges on SOI substrate adhered on the outer surface of a steel plate is not a precise flexible stress sensor, but a means of estimation in strain/stress and pressure. Another report on a fully packaged strain sensor device based on a single ZnO piezoelectric fine-wire (NWs, microwires) gives us a vivid description of the real flexible stress sensors.¹³⁹ As shown in Fig. 9a, the flexible and optically transparent strain sensor

device was fabricated by bonding a ZnO piezoelectric fine-wires laterally on a polystyrene (PS) substrate. Silver paste was applied at both ends of the ZnO wires to fix its two ends tightly on the PS substrate while serving as the source and drain electrodes. And a thin layer of polydimethylsiloxane (PDMS) was introduced to package the device. I-V behaviors of the sensor device were measured under various strains as shown in Fig. 9b. We can see that the I-V curves shift upward with tension strain and downward with compressive strain under various strains. Besides, current response of the sensor over many cycles of repeatedly compressing and stretching were also tested and the results were recorded in Fig. 9c. Fig. 9d is the partial enlarged drawing. The highly regular response curves indicate the high reproducibility and good stability of this kind of flexible sensor device. Gauge factor, which is the key parameter for a practical strain sensor, defined as $[\Delta I(\epsilon)/I(0)]/\Delta\epsilon$ where $\Delta\epsilon$ and $\Delta I(\epsilon)$ are the amount of variation change of strain and the corresponding current. The highest gauge factor demonstrated for this kind of flexible stress sensor device is 1250, far exceeding the conventional doped-Si strain sensor (~ 200). The outstanding performance of this flexible strain sensor based on ZnO nano/microwires shows its good application future in strain and stress measurements in the fields of science and technology.

3.3.3 Artificial skins

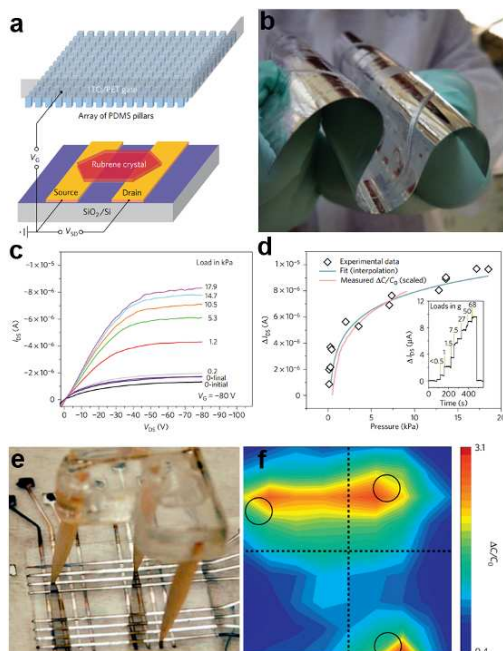


Fig. 10. (a) Schematic of the pressure-sensitive organic field-effect transistors device that using the microstructured PDMS film as the dielectric layer. (b) Optical image of the aluminum-coated microstructured PDMS film, indicating the high flexibility of the dielectric layer film. (c-d) Pressure response of the pressure-sensing organic single-crystal transistors based on the microstructured PDMS dielectric layer. (e) Flexible 8×8 pixel pressure sensor arrays fabricated by sandwiching the microstructured PDMS film between two PET substrates. (f) The pressure response to an above-placed tripod. Reprinted with permission from ref. 140 © 2010, Macmillan Publisher Ltd.

Touch is an efficient way that we interact with our surrounding environment and skin is the natural interfaces between man and

other things. Emulation of the stress senses by artificial means is a great challenge as well as an intriguing task. By applying a certain pressure over a stress sensor, a corresponding current or voltage signal could be obtained. So it is easy to imagine a kind of primitive artificial skin that composed of neatly arranged stress sensor arrays, in which every single pressure sensing pixel is independently driven. However, the flexibility is still the most basic demand of the artificial skins. This requires that we fabricate fully flexible electronic stress sensor arrays or at least sensor arrays based on some flexible substrate. As recently reported by Bao, et al., flexible pixel-type pressure-sensor arrays with high sensitivity and very short response times have been designed.¹⁴⁰ In their work, organic field-effect transistors (OFETs) including a cleverly designed thin, regularly structured rubber (PDMS film with 3-D microstructures) served as the active elements in press sensor devices. Fig. 10a-b shows the layout of the organic FETs employing PDMS film as the dielectric layer. Under different applied pressure, the organic single-crystal transistors have different output currents (Fig. 10c). The change in current is proportional to the measured relative change in capacitance, which depends directly on applied pressure (Fig. 10d). A primitive capacitive matrix-type pressure sensor was also designed to prove the possibility for use in multi-touch devices of this flexible electronic stress sensor. Details of the structure and its performance are shown in Fig. 10e-f.

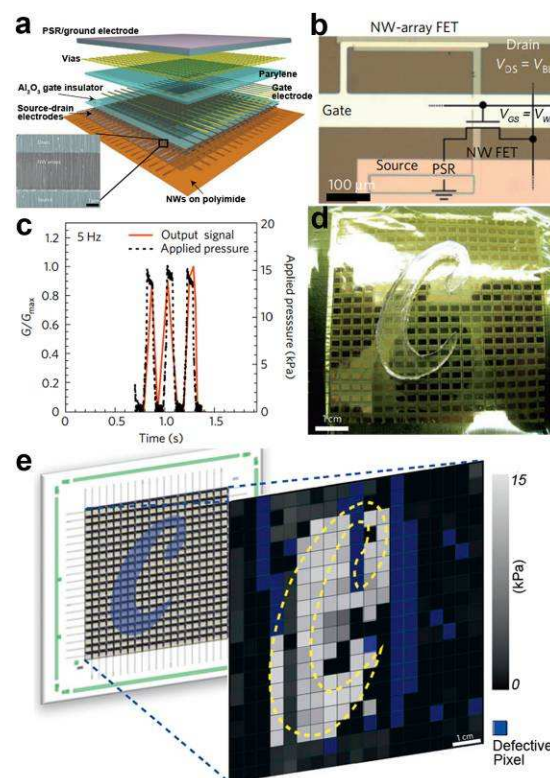


Fig. 11 (a) Schematic of the passive and active layers of NWs based artificial skin. (b) Optical image of the individual stress sensing pixel. (c) Time dependent output signal for an applied pressure frequency of 5 Hz. (d) As-fabricated 19×18 pixel array artificial skin with a 'C' shaped PDMS mould placed on the top for applying pressure. (e) Corresponding two-dimensional output signal profile. Reprinted with permission from ref. 141 © 2010, Macmillan Publisher Ltd.

Parallel NW arrays were proven to be promising candidates for flexible and robust artificial skin, as reported by Takei *et al.*¹⁴¹ In their work, macroscale ($7 \times 7 \text{ cm}^2$) integration of parallel NW arrays as the active-matrix backplane of a flexible pressure-sensor array were reported, as shown in Fig. 11a and 10b. A laminated pressure-sensitive rubber (PSR) is used as the sensing element and the source electrodes of printed Si/Ge NW-array based FETs (Inset of Fig. 11a) are connected to drive the PSR. With variations of external pressure, the conductance of PSR rises or falls, leading to the different modulation index of the NW FETs and eventually bring the specific output signal of the pixel. By setting a certain frequency of the applied pressure, the corresponding time dependent output electrical signal of a pixel could be obtained. Fig. 11c shows the conductance-pressure profile with a frequency of 5Hz, indicating the fast and stable response of this stress sensing unit. Finally, a 19×18 pixels array based artificial skin was successfully fabricated, as shown in Fig. 11d. A normal pressure of $\sim 15 \text{ kPa}$ was applied on the surface of a 'C' shaped PDMS film which was covered onto the artificial skin. By measuring the conductance of each pixel and introducing normalizations, the authors gave the two-dimensional intensity profile (Fig. 11e). The contrast represents the normalized output signal, with the blue pixels representing the defective points. The character 'C', corresponding to the applied pressure area illustrate the stable response of this flexible artificial skin. Uniform assembly of ordered Ge/Si NW arrays ensured the outstanding mobility of ($\sim 20 \text{ cm}^2/\text{Vs}$) NW-array FETs and granted a superb mechanical flexibility of the flexible artificial skin. NW also has the single-crystalline nature, which could help to a low-voltage operation mode for the sensor circuitry. All these attributes make the parallel NW arrays ideal choice for more sophisticated artificial skin.

Although the above work demonstrated the fulfillment of artificial skin with NW arrays, it only involved the integration of pressure sensors with an NW based electronic readout circuit. It was very inconvenient to obtain an intuitive grasp on the performance of the flexible artificial skins, as output of each pixel was individually measured then statistically analyzed. A great progress was recently obtained by Wang, *et al.*, who designed a user-interactive artificial skin which not only spatially maps the applied pressure but also provides an instantaneous visual response through a tricolour OLED pixels array.¹⁴² This artificial skin basically consists of three parts, namely pressure-sensitive rubber, active-matrix backplane circuitry and an OLED arrays. As shown in Fig. 12a, each sensing and display pixel consists of a TFT, an OLED and a PSR integrated vertically on a polyimide substrate. The enlarged optical micrographs of one pixel is shown in Fig. 12c, where we can see that the drain of the TFT is connected to an ITO pad that serves as the anode electrode for the corresponding OLED, while the cathode of each OLED is connected to the ground through the PSR. Fig. 12b illustrates an entire 16×16 pixels array of pixels, in which the scan lines (5/35 nm Ti/Au back-gate electrodes) and data lines (0.5/40 nm Ti/Pd source-drain contacts) are connected to 5 and 10 V voltage, respectively, as shown in Fig. 12d. In Fig. 12e, a letter shaped PDMS slabs was placed onto the PSR and uniform external force was applied on the PDMS slabs. The conductivity of the PSR increased accordingly and subsequently resulted in the underlying

OLED turning on. A uniform performance of each TFT and single-pixel OLED allowed the pressure signal to be both spatially mapped and visually seen, as corresponding C-, A- and L-shaped bright light emitting area were clearly recognized on the OLED panel. (Fig. 12e, right) Besides, the color of the OLED can be effectively tuned by applying different emissive layer materials and the brightness of each OLED can also be sensitively controlled by the magnitude of the local pressure. Although the spatial resolution is far from practical application, this flexible artificial skin still demonstrated the practicability of user-interactive sensing system. By further improving the pixel integration level and using multiple sensor components, a superior kind of artificial skin that enables more sophisticated bionic operations can be successfully planned.

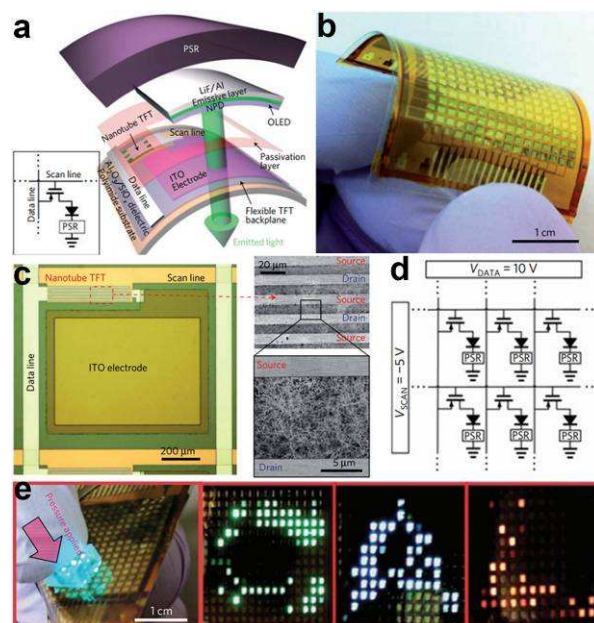


Fig. 12 (a) Schematic illustration of the user-interactive artificial skin. (b) Photograph of a fabricated device (16×16 pixels) artificial skin. (c) Enlarged view of the active area. (d) Circuit schematic of the artificial skin matrix. (e) As-fabricated 16×16 pixel array artificial skin with a 'C/A/L' shaped PDMS slabs placed on the top for applying pressure. Reprinted with permission from ref. 142 © 2013, Macmillan Publisher Ltd.

3.4 Display devices

As one of the important display components, the light emitting diode developed rapidly in recent years. NWs based on various semiconductors offer the added advantage of high material quality leading to improved device performance. Basically, research in the area of NW based display component was focused on two sides.

On one hand, semiconductor NWs was used as the optical active component in display devices. Individual gallium nitride (GaN) NW has been configured as UV-light-emitting diodes on flexible plastic substrates by Lieber's group.¹⁴³ In this report, the authors assembled crossed n-type GaN NWs and p-type Si NWs onto plastic substrate to form a flexible crossed-NW LEDs, as shown in Fig. 13a-b. This kind of n-GaN/p-Si crossed diodes not just showed stable emission (Fig. 13c), it could also maintain their emissive properties upon repeated cycles of bending. In

another work, vertically oriented ZnO NWs also fabricated into a highly flexible light-emitting device.¹⁴⁴ From the design scheme in Fig. 13d, we could see that the flexible LED was composed of four layers, namely, supporting (PET/ITO) substrate, vertically oriented ZnO NWs layer, insulating polystyrene (PS) film and the hole-injection anode layer respectively. In particular, the hole-injection anode layer consisted of a thin poly (3,4-ethylenedioxythiophene) poly(styrenesulfonate) (PEDOT:PSS) layer and an evaporated Au film. Fig. 13e-f gave the overall image of the active ZnO NWs layer. All NWs showed a uniform size with typically $\sim 2\mu\text{m}$ in length and 70-120 nm in diameter. With or without Al doped, this diode structure both showed excellent optical emission performance in the range of 500-1100 nm (Fig. 13g). These results suggest that semiconductor NWs could serve as the high-performance building blocks for the future lightweight display devices.

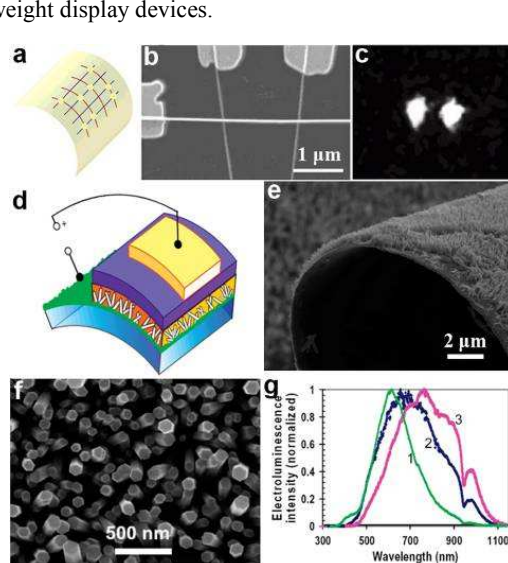


Fig. 13 (a) Schematic and (b) SEM image of a crossed-NW LED array on a flexible plastic substrate, in which p-SiNWs are vertically aligned and GaN NW is horizontally aligned. (c) Electroluminescence (EL) images of localized emission from forward-biased Si-GaN junctions. Reprinted with permission from ref. 143 © 2003, American Chemical Society. (d) Scheme for a flexible LED structure consisting of vertically oriented ZnO NWs grown on a polymeric ITO-coated substrate. (e-f) SEM images of the ZnO NWs grown on a planar transparent substrate and on a bent Au film, respectively. (g) Normalized electroluminescence spectra versus wavelength based on various LED structures. Reprinted with permission from ref. 144 © 2008, American Chemical Society.

On the other hand, semiconductor NWs was used as the transistor driving circuitry. NW transistor driving circuitry is of particular interest for future display devices because of its high carrier mobility, its optical transparency, as well as their mechanical flexibility. Zhou et al. reported high-performance arsenic (As)-doped indium oxide (In_2O_3) NWs for transparent active-matrix organic light-emitting diode (AMOLED) displays.⁶ Thin-film transistors (TFTs) based on As- In_2O_3 acted as the key components of the driving circuitry. The synthesized As-doped In_2O_3 NWs was shown in Fig. 14a, which have high electron mobility of $\sim 1490\text{ cm}^2/\text{Vs}$. The as-designed TFTs can be used as driven circuit to control a variable-intensity OLED, as shown in the inset of Fig. 14b. Regulating the input voltage could efficiently control the light intensity of the OLED. Fig. 14c is the circuit diagram that indicates the physical layout of the

connections for the seven-segment AMOLED display. The most important components of this circuitry were the switching transistors (T_1), driving transistors (T_2), and one storage capacitor (C_{st}). They were introduced here to select a specified pixel, control the current and store data during one period for time-varying operations, respectively. This fully integrated seven-segment AMOLED display was proved to have a good transparency of 40%. As shown in Fig. 14d. Background image could be partly seen through the AMOLED display arrays. Optical images of the seven-segment pixels with lighted numerical digits (Fig. 14e-g) indicated the outstanding and stable performance of the NWs transistor driving circuitry. By changing the ITO glasses with the PET substrate, the authors further proved the successful fabrication of flexible SWNT transistors for LED driving circuitry.⁴⁹

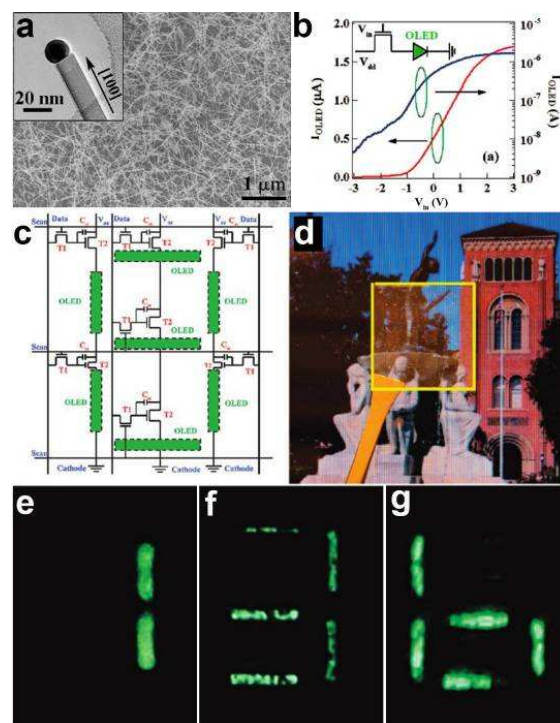


Fig. 14 (a) SEM image of As- In_2O_3 NWs. (b) output current through the loaded phosphorus OLED (I_{OLED}) versus V_{in} with V_{dd} at 5.0 V in linear scale (red line) and log scale (blue line), respectively. (c) Circuit diagram of seven-segment AMOLED display unit. (d) Optical photograph of fully transparent AMOLED display driving circuitry. (e-g) The seven-segment AMOLED display unit displays numbers 1, 3, and 6, respectively. Reprinted with permission from ref. 6 © 2009, American Chemical Society.

3.5 Memories and logic gates

Over the past several years, semiconductor NWs have also represented attractive building blocks for memories and logic gates, which are essential component for the next generation circuits. Traditional memories and logic gates based on silicon has greatly promoted the development of the very large scale integrated circuit (VLSI). However, in terms of flexible devices for example that designed to mount on human skin or planted into internal organs, constraint of traditional electronic units would certainly limit their potential applications. So fully flexible memories and logic gates have been greatly welcomed by

scientific researchers for NW based electronic devices.

Lieber's group first reported the monolithic integration of individual and parallel arrays of germanium/silicon (Ge/Si) core/shell NWs as multilayer flexible circuits.¹⁴⁵ As shown in Fig. 15a and Fig. 15b, the final circuit consists of a lower layer of PMOS inverters and an upper layer of floating gate memory elements. From the input-output characteristics of the lower layer of PMOS inverter (Fig. 15c), it was found that this inverter exhibited p-type transfer characteristics with a maximum voltage gain of 3.5. Fig. 15d is the AC inverter characteristics of the lower layer of PMOS inverters when driven by a 50 MHz sine wave supply of 4 V. At a frequency of 50 kHz, the input signals are ideally inverted to the output signals without any loss. Fig. 15e and Fig. 15f are the current vs voltage sweeps recorded on the upper layer of floating gate memory elements. A large hysteresis (i.e. memory window) and stable writing and erasing operation can be observed respectively, indicating the good memory retention of the floating gate memory elements.

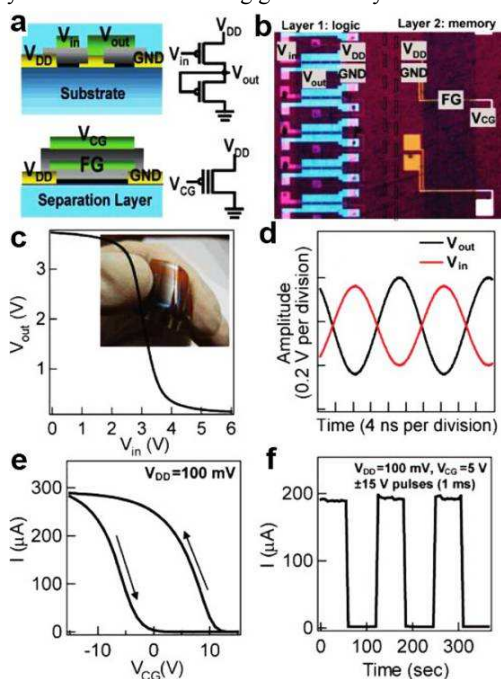


Fig. 15 (a) Schematics and circuit diagrams of inverter (top) and floating gate memory (bottom) elements. (b) Optical image of inverters (layer 1) and floating gate memory (layer 2) on Kapton. (c) DC inverter characteristics. (d) AC inverter characteristics. (e) Hysteresis in current-voltage characteristics of a memory layer element. (f) Switching characteristics of memory at $V_{CG} = 5$ V with ± 15 V pulses (pulsing time, 1 ms). Reprinted with permission from ref. 145 © 2007, American Chemical Society.

Flexible logic gates were also fabricated on the base of well aligned NWs that generated by top-down fabrication steps.¹⁴⁶ By using anisotropic chemical etching steps, Rogers *et al.* have once obtained GaAs nano/microwires with triangular cross sections from GaAs wafers. A slightly oxidized PDMS stamp was used to transfer the GaAs wire arrays from the original base onto a PET/PU (polyurethane) substrate (Fig. 16a). Simple circuits consist of various logic gates and individual MESFETs on a PET substrate is shown in Fig. 16b-c. Logic functions, such as NOR and NAND gates can be performed by this flexible logic circuits. For example, Fig. 16d-e shows the scheme of combining two

GaAs wire switching transistors with another GaAs wire load transistor to yield NOR logic functions, as logic status of V_{out} can only be logic 1 (high positive output voltage) when both inputs are logic 0 (at high negative voltages). Fig. 16f-g shows the optical image of circuit diagrams as well as the voltage transfer characteristics of the NAND gate, respectively. It can be seen that the flexible NAND gate also shows very stable logic operation performance. Furthermore, Rogers and his mates have reported a medium-scale integrated digital circuit composed of up to about 100 SWNT transistors fabricated on flexible plastic substrate.¹⁴⁷ This flexible digital circuit could be used to decode a binary-encoded input of four data bits into sixteen individual data output lines. This outstanding ability suggests that well-designed flexible integrated circuits based on NWs could be applied widely in many areas where conventional, rigid circuits cannot meet requirements, for example implantable electronics and prosthetics *et al.* in the near future.

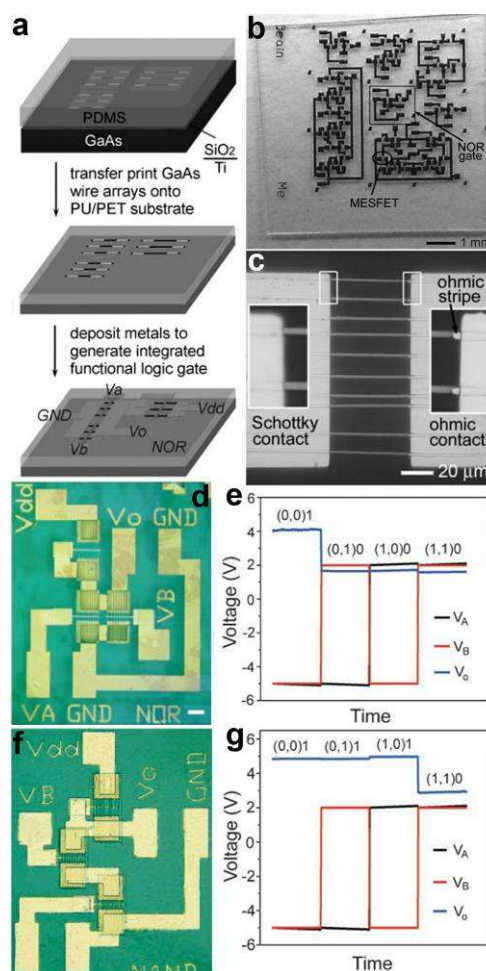


Fig. 16 (a) Transfer print process of GaAs wires and logic device fabrication process. (b) Optical images of various logic gates and individual MESFETs fabricated on the PET substrates. (c) Magnified optical micrograph of an individual Ti/n-GaAs Schottky diode on the PET sheet. (d-e) Optical images and input-output characteristics of a NOR gate. (f-g) Optical images and input-output characteristics of a NAND gate. Reprinted with permission from ref. 146 © 2006, WILEY-VCH.

4 NW flexible energy conversion and storage devices

Accompanied with the development of flexible electronics, great interest has been aroused in integral flexible/bendable electronic equipment such as wearable devices, rollup displays and bendable mobile phones. However, the current energy storage devices containing lithium ion batteries and supercapacitors are usually too heavy, rigid and bulky to match particular requirements of flexible electronics. Therefore, the trend in the next generation of energy storage devices development is to realize light, flexible and small units with shape-conformability, aesthetic diversity and excellent mechanical properties. NWs with high aspect ratio, fast charge transfer pathways and stable frameworks have attracted increasing research interest in the area of energy conversion and storage. In this section, we review some recent advances that NWs have made in the field of lithium ion batteries (LIBs), supercapacitors (SCs), solar cells, and generators.

4.1 Lithium ion batteries

Among the newly emerged energy storage devices, lithium ion batteries (LIBs) are one of the most popular candidates due to their relatively high energy density, long cycling life, good power performance and low cost.¹⁴⁸⁻¹⁷⁸ For the LIBs, the charges stored are mainly contributed by the intercalation of Li^+ on the surface and in the bulk of the active materials, delivering higher energy density (120-180 Wh/kg) than the other energy storage devices.¹⁴⁸ NWs with highly elastic structure are demonstrated appropriate for the novel flexible LIBs, which are in urgent

demands to meet the development and promotion of flexible electronics. Recently, several excellent comprehensive reviews were given to introduce the fast development of flexible LIBs thus we will not give details, but brief introduction to this area.¹⁷⁹⁻¹⁸²

Planar type flexible LIBs is one of the most important and earliest developed battery. This kind of flexible LIBs has the features of very thin thickness, light weight, good energy density and power density, and excellent cycling stability. One good example is the flexible planar LIBs with 3D hierarchical ZnCo_2O_4 NW arrays grown on carbon cloth as the flexible electrodes.¹⁶⁷ As shown in Fig. 17, the 3D nanostructure exhibits a distinct plateau between 0.8 and 1.2 V in the voltage window of 0.01–3.0 V and only 16.5% decay of initial capacity (1530 mAh/g) after 100 cycles (Fig. 17c). The specific capacity almost maintains constant in the range of about 1200-1340 mAh/g with 99% capacity retention from 3 to 160 cycles. Fig. 17d illustrates the typical voltage profiles of the flexible battery device composed of ZnCo_2O_4 /carbon cloth as anode and LiCoO_2 /Al foil as cathode by bending it from different directions for hundreds cycles. The constant capacity even after 120 cycles of bending reveals that the electrical stability of the fabricated flexible full battery is hardly affected by external bending stress. The good adhesion and electrical contact between the NWs and carbon cloth, the facile diffusion of the electrolyte and accommodation of the strain induced by the volume change and the 3D hierarchical nanostructures resulted in better performance of the flexible battery. An enhanced power density was achieved once urchin-like ZnCo_2O_4 NWs was used.¹⁷²

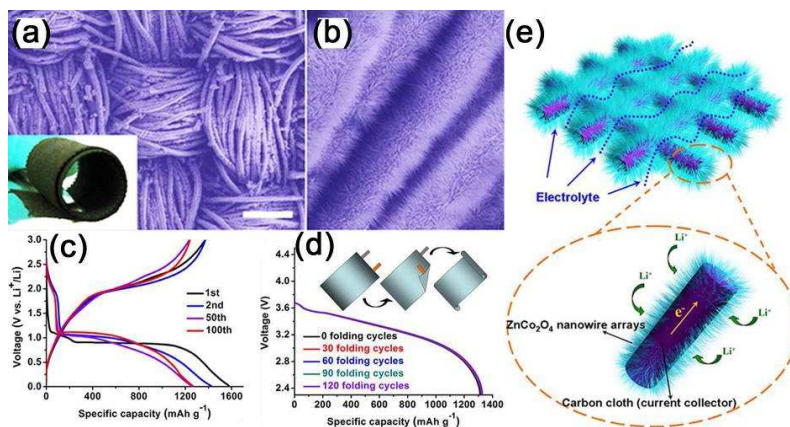


Fig. 17 (a, b) Typical FESEM images of the ZnCo_2O_4 NW arrays growing on carbon cloth at different magnifications. (c) Typical voltage versus specific capacity profiles for the first, second, 50th, and 100th discharge and charge-cycle. (d) Typical voltage versus specific capacity profiles for the first, second, 50th, and 100th discharge and charge-cycle after 0, 30, 60, 90, and 120 folding cycles. (e) Schematic representation and operating principles of rechargeable lithium-ion battery based on ZnCo_2O_4 NW arrays/carbon cloth. Reprinted with permission from ref. 167 © 2012, American Chemical Society.

Besides ZnCo_2O_4 NWs, other metal oxide nanowires were also used to fabricate flexible LIBs. Although this type of planar flexible LIBs shows many advantages compared with the conventional rigid LIBs, it still has several drawbacks. For example, the size of planar flexible LIBs is still quite large and the device is still too thick, which makes it unfit for integration with other flexible electronic or optoelectronic devices, especially in the case of on-chip integration for microelectronics applications. Besides, this kind of planar flexible LIBs cannot stand large degree of curving or bending, which also makes it

impossible for real flexible electronics applications.

One solution to overcome these problems is to develop ultra-small and stretchable LIBs.¹⁸³ Stretchability represents a rigorous challenging of mechanical stability. The stretchable devices must bear large strain deformation, and large shape deformation, including not only bending, but also twisting, stretching, compressing and others. Recently, Rogers et al. developed a very fancy type of highly stretchable LIBs with the active materials segmented design, and unusual 'self-similar' interconnect structures between them. The stretchable LIB was fabricated on

thin silicone elastomers as substrates, as illustrated in Fig. 18a. As a result, the as-fabricated LIB obtains a stretchability up to 300%, and it still maintains a capacity of as high as 1.1 mA h cm⁻² at a rate of C/2. Although the output power of the battery decreased slightly with strain resulted from the increased internal resistances with strains at these large levels, surprisingly, the stretchable battery could turn on a commercial LED even when it was stretched by up to 300%, as can be seen in Figure 18b and c. The high stretchability of the fabricated battery satisfies the requirements for many applications that are being contemplated for stretchable electronics.

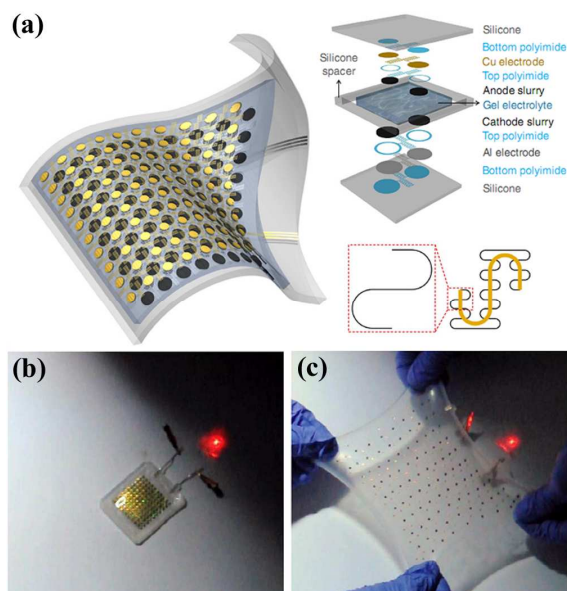


Fig. 18 (a) Schematic illustration and exploded view layout of a completed stretchable LIBs. (b, c) Lighting a red LED without and with

15 strain. Reprinted with permission from ref. 183 © 2013, Macmillan Publisher Ltd.

Although great progresses have been obtained in flexible LIBs, the following several things should be considered before their real applications in flexible electronics. First, both the energy density and power density should be further improved to make them comparable with the conventional rigid LIBs. Second, it is quite important and sometime essential to fabricate ultra-small batteries to realize chip-level integration with flexible electronic or optoelectronic devices. Third, more delicate device should be designed in case of special applications.

4.2 Supercapacitors

Supercapacitors (SCs), also known as electrochemical capacitors or ultracapacitors, are another kind of vital energy storage devices because of the long cycle life (>10⁵ cycles), high power density (>10 kW/kg) and high rate capability with fast charge-discharge within seconds. Similar with the configuration of LIBs, a SC is also composed of an anode, cathode, separator and electrolyte. The working mechanism of SCs can be classified into electrical double layer capacitors (EDLCs) and the pseudocapacitors.¹⁸⁴⁻¹⁸⁵ Since both the EDLCs and the pseudocapacitors are surface electrochemical related devices, high surface area electrode materials are necessary in SCs, fitting well with the features of NWs. Similar with the construction of flexible LIBs, several kinds of flexible SCs are demonstrated based on NWs (carbon materials, transition metal oxides and conducting polymers), including the paper-like SCs, transparent SCs, woven SCs, micro-SCs and fiber SCs, which will be discussed in sequence in the following sections.

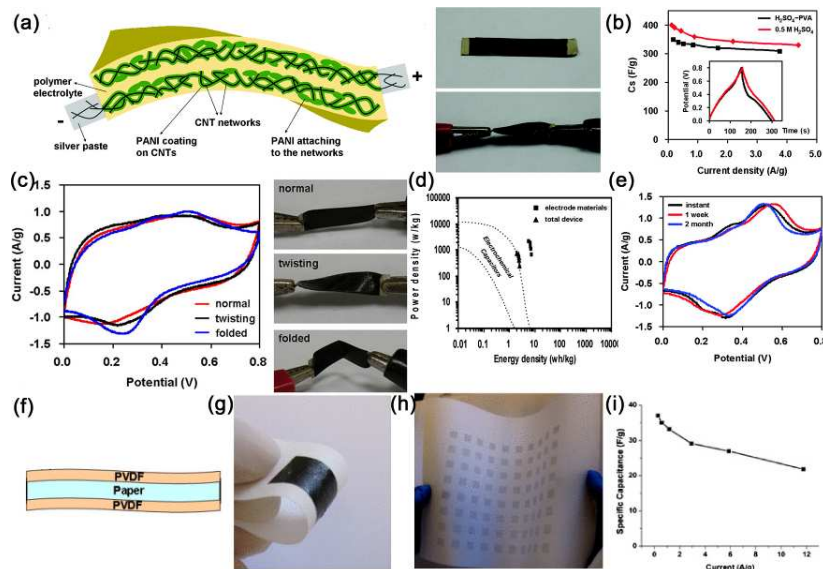


Fig. 19 (a) Schematic illustration of the PANI/CNT nanocomposite electrodes well solidified in the polymer gel electrolyte and digital pictures that show the all-solid-state device (size ~0.5 cm x 2.0 cm) under normal condition (top) and its highly flexible (twisting) state under electrochemical measurements (bottom). (b) Comparison of discharge abilities of the flexible PANI/CNT nanocomposite thin film electrodes in the H₂SO₄-PVA gel electrolyte and in the 0.5 M H₂SO₄ aqueous solution. The inset in (b) shows one cycle of galvanostatic charge-discharge curves at 1 A/g. (c) Comparison of CV curves at 5 mV/s for the all-solid-state device tested in the normal, twisting and even folded condition, respectively. (d) Ragone plots for the electrode materials and for the entire all-solid-state device. (e) Time life stability of the device. Reprinted with permission from ref. 198 © 2010, American Chemical Society. (f) Schematic of Xerox brand printer paper treatment with PVDF. (g) A photo of a Meyer rod-coated supercapacitor on Xerox paper. (h) A photo of ink-jet

printed supercapacitor on Xerox paper. (i) Specific capacitance at different current density. Reprinted with permission from ref. 201 © 2010, AIP Publishing LLC.

4.2.1 Paper-like Supercapacitors

Besides high flexibility, paper-like SCs also exhibit ultrathin and lightweight properties. Free-standing CNT papers possess high conductivity and excellent flexibility, which can serve as both electrode materials and current collectors. However, the free-standing CNT paper with connecting bundles usually suffer a low specific surface area and thus a poor capacitive performance (less than 100 F/g), which limits the energy density of the SCs.¹⁸⁷⁻¹⁸⁹ There are two ways to improve the performance of free-standing CNT papers. The first one is to incorporate active carbons and etched carbon materials.^{186,190-192} For example, Zheng et al. increased the specific surface area of a hierarchical CNT film from 670 to 871 m²/g by using CO₂ etching method, reaching a maximum value of 267.6 F/g after loading 5 wt% of etched CNT into the ultralong CNT networks. The second way is to form hybrid transition metal oxides/CNTs or conducting polymers/CNTs to obtain higher energy densities.¹⁹³⁻²⁰⁰ Liu et al. designed flexible and ultrathin all-solid-state supercapacitors with two slightly separated PANI/CNT nanocomposite electrodes well solidified in the H₂SO₄-polyvinyl alcohol (PVA) gel

electrolyte.¹⁹⁸ Fig. 19a displays the configuration of the as-fabricated SC. The free-standing CNT networks, whose electrical conductivity is as high as to 15000 S/m, served as the scaffold for incorporation of polyaniline and current collectors. The volume density of the CNTs was only 30%, leaving 70% of the total networks in the form of porous structure. Even though the thickness of the device was estimated to be only 113 μm, the entire device shows superior mechanical flexibility. At 1.0 A/g, the discharge specific capacitance of the flexible device is 332 F/g based on the total mass of the device, which is only 7.8% smaller than the one in 0.5 M H₂SO₄ solution (360 F/g) (Fig. 19b). A high energy density of 7.1 wh/kg and a high power density of 2189 w/kg were achieved, which is far superior to those of current conventional supercapacitors (Fig. 19d). After 1000 charge-discharge cycles, the device shows a good cycling stability with only 8.1% decay and a stable Coulombic efficiency ranging from 95.2% to 102.8%. During the time stability test displayed in Fig. 19e, the capacitance shape and redox peaks were well retained after 1 week and even 2 months, leading to a much stable device.

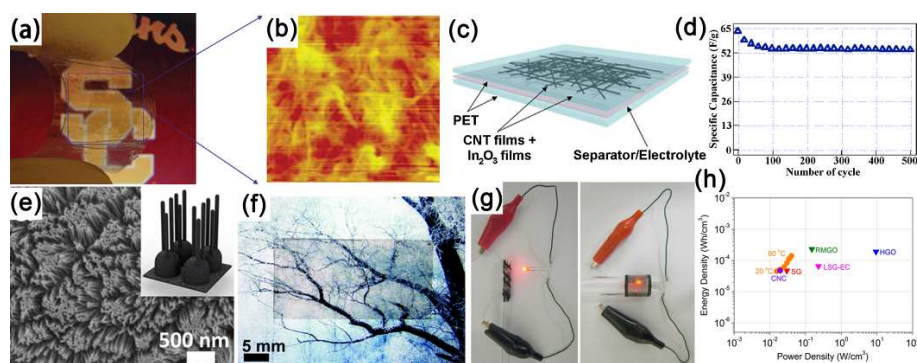


Fig. 20 (a) Photograph of a flexible and transparent supercapacitor fabricated using CNT films. (b) AFM image of entangled CNT networks sitting on a transparent PET substrate. (c) Schematic of a flexible and transparent supercapacitor. The gray color represents a Nafion film as separator between two In₂O₃ NWs/CNT heterogeneous film electrodes. (d) Cycle-life data of In₂O₃ NWs/CNT heterogeneous film electrochemical capacitor measured at 0.5 A/g. Reprinted with permission from ref. 206 © 2009, AIP Publishing LLC. (e) SEM images of branched nanocup film, where short carbon nanotubes (25 nm in diameter and 330610 nm in length) are branched from the bottom of a nanocup. (f, g) Transparent and flexible nature of the supercapacitor devices. (h) CNC devices are compared with various energy storing devices by the Ragone plot that is the values of energy density for power density. (SG: single layer graphene, RMGO: reduced multilayer graphene oxide, HGO: hydrated graphitic oxide, LSG-EC: laser-scribed graphene electrochemical capacitor). Reprinted with permission from ref. 208 © 2012, Macmillan Publisher Ltd.

Another kind of paper-like supercapacitors are fabricated by coating the conductive and electroactive CNTs or semiconductor NWs onto paper substrates.^{161,163,201-204} Among the reported achievements, Cui's group has dedicated a lot of efforts on the paper-like supercapacitors by using the low-cost Xerox paper as the substrates. For instance, Cui et al. report carbon nanotube thin film-based supercapacitors fabricated with printing methods, where electrodes and separators are integrated into single sheets of commercial paper.²⁰¹ Before coating the SWCNT ink on to the paper, the paper substrates were first treated with polyvinylidene fluoride (PVDF) to prevent the penetrate of ink into the paper. The schematic illustration is presented in Fig. 19f. Fig. 19g shows a printed supercapacitor using the Meyer rod coating method. For the large scale fabrication, an ink-jet printer can be utilized to print any patterns (Fig. 19h). Based on the voltage profile and the mass density of SWCNT, the specific capacitance is calculated to

be 33 F/g (Fig. 19i) at a specific power of 250 000 W/kg. Due to the lightweight SWNT films and the absence of heavy metals, the capacitance of assembled device could be greatly improved when compared with traditional supercapacitors.

4.2.2 Transparent Supercapacitors

Flexible and transparent supercapacitors have recently attained great research interest to drive the flexible and transparent electronics such as transparent and flexible active matrix organic light-emitting diode display which may find applications in heads-up display, automobile wind-shield display, and conformable products.²⁰⁵ NW based flexible and transparent electrodes were demonstrated by depositing the NWs (CNTs, carbon nanocup arrays, polyaniline NWs and In₂O₃ NWs et al.) onto the flexible and transparent substrates.²⁰⁶⁻²¹⁰ Chen et al. demonstrated a supercapacitor with the features of optical

transparency and mechanical flexibility using In_2O_3 NWs/CNT heterogeneous film, as shown in Fig. 20a-d.²⁰⁶ The device delivered a high specific capacitance of 64 F/g and good stability.

More recently, Jung et al. constructed mechanically flexible and optically transparent thin film solid state supercapacitors by assembling nano-engineered carbon electrodes.²⁰⁸ Through the control of nanopore dimension in anodic aluminum oxide (AAO) templates and CVD conditions, precisely tailored carbon nanocups can be fabricated, seeing from Fig. 20e. The as-fabricated electrode is highly conductively (117 S/m) and transparency. After being sandwiched by polyvinyl alcohol-phosphoric acid gel electrolyte, the transparent and highly flexible supercapacitors are demonstrated (Fig. 20f and g). With the increasing measured temperature, a high areal capacitance of 1220 $\mu\text{F}/\text{cm}^2$ was obtained at 80 °C, which is almost three times than that (409 $\mu\text{F}/\text{cm}^2$) at room temperature. The Ragone plot is shown in Fig. 20h. The volumetric peak power and energy densities of the branched carbon nanocap based supercapacitors are 19 mW/cm^3 and 47 mWh/cm^3 respectively, which is similar to some high performance graphene-based supercapacitors.²¹¹

4.2.3 Wearable Supercapacitors

Smart textiles have unique functions such as thermal energy conversion, energy storage, sensors and communication etc.²¹² Among them, wearable supercapacitors are considered as an important element to drive the other textile electronics. So far, much progress has been achieved on the design of wearable supercapacitors and NWs have contributed a lot to function as the

conductive and electroactive materials. The substrates used in the wearable supercapacitors include the carbon cloth,²¹³⁻²¹⁶ cotton fabrics,²¹⁷⁻²¹⁹ non-woven cloth and so on.^{220,221}

Carbon cloth, as flexible, conductive and stable substrates, has attracted much interest to be used as the current collectors in flexible supercapacitors. Our group has devoted some efforts on the development of flexible SCs by using carbon cloth current collectors to support NWs.^{213,216} For example, we developed an asymmetric supercapacitors (ASCs) based on acicular Co_9S_8 nanorod arrays as positive materials and Co_3O_4 @ RuO_2 nanosheet arrays as negative materials.²¹³ Acicular Co_3O_4 nanorod arrays were first grown on carbon cloth, acting as templating for further Co_9S_8 nanorod arrays growth or RuO_2 nanosheets deposition (Fig. 21a,b). The schematic illustration of the as-fabricated ASC is shown in Fig. 21c. Remarkably, the as-fabricated ASCs could be cycled reversibly in the range of 0-1.6 V in aqueous electrolyte (LASC) and solid-state (SASC) electrolyte. The performance of SASC was preserved after being bended and twisted, demonstrating the desirability of carbon cloth-based current collectors (Fig. 21d). Both capacitors reveal excellent rate performance through five steps of charge/discharge rates changed successively from 2.5 to 50 mA/cm^2 . Moreover, high volumetric capacitance of 4.28 F/cm^3 for SASC remained 90.2% after 2000 charge/discharge cycles. Electrochemical performance with an energy density of 1.44 mWh/cm^3 at the power density of 0.89 W/cm^3 for SASC was demonstrated.

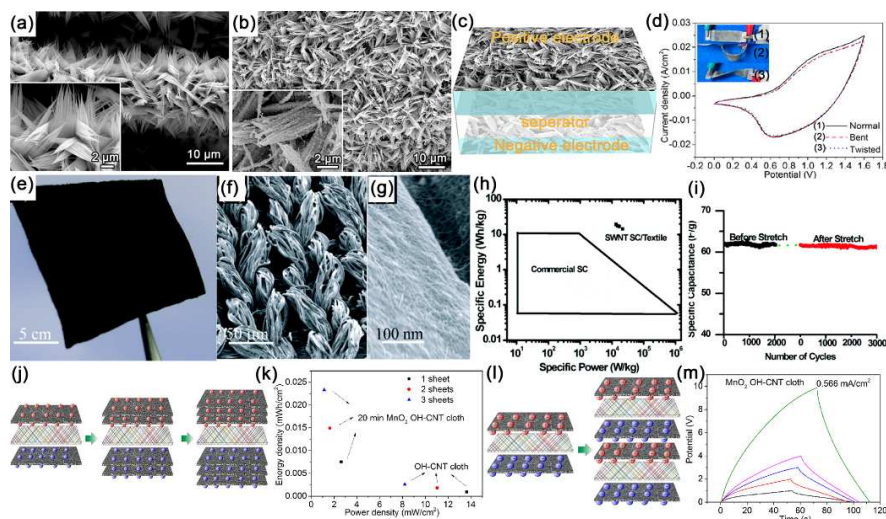


Fig. 21 (a, b) SEM images of Co_3O_4 and Co_9S_8 acicular nanorod arrays grown on carbon cloth. (c) Schematic illustration of the asymmetric supercapacitors utilizing Co_9S_8 -carbon cloth as positive electrode and RuO_2 -carbon cloth as negative electrode. (d) CV curves of the ASC tested under normal, bent and twisted conditions. Reprinted with permission from ref. 213 © 2013, American Chemical Society. (e-g) Photograph and SEM images of CNT coated cotton cloth. (h) Ragone plot of commercial SCs and SWNT SC on porous conductors including all the weight. (i) The specific capacity for a stretchable SC before and after stretching to 120% strain for 100 cycles. The current density is 1 mA/cm^2 . Reprinted with permission from ref. 217 © 2010, American Chemical Society. (j) Schematic illustration of the laminated structure of fabric SC. (k) Ragone plot of the laminated capacitors. (l) Schematic illustration of the tandem structure of fabric SC. (m) Galvanostatic charge/discharge curves measured at 0.566 mA/cm^2 for tandem MnO_2/CNT fabric SC with the number of units of 1, 2, 3, 4, 10 respectively. Reprinted with permission from ref. 220 © 2013, Wiley-VCH.

Low-cost, flexible, stretchable and lightweight cotton cloth and non-woven cloth were also proved to be ideal substrates for wearable supercapacitors. Cui's group conformally coat single-walled carbon nanotubes (SWNTs) on cotton cloth to make porous conductors.²¹⁷ As shown in Fig. 21e-g, the uniformly coated SWNTs make these textiles highly conductive with sheet

resistance less than 4 Ω/sq . Supercapacitors made from these conductive textiles with large CNT loading mass (up to 8 mg/cm^2) showed high areal capacitance, up to 0.48 F/cm^2 and good cycling stability (<2% decrease after 130000 cycles). In the Ragone plot (Fig. 21h), the mass of electrode materials (~16 mg/cm^2), the cotton (~24 mg/cm^2), electrolyte (~6 mg/cm^2), and

separator ($\sim 2 \text{ mg/cm}^2$) were all included in the complete SC device, which reaches a high energy density of 20 Wh/kg at a specific power of 10 kW/kg . When substituting the cotton cloth with stretchable fabrics, a flexible and stretchable SC is also feasible, showing excellent stability even after thousands of cycles (Fig. 21i).

The current generation of energy storage systems often occupy more space than the electronic devices that they power. Therefore, the areal capacity and output voltage are key factors and can be tuned by textile electrodes. Recently, building on non-woven cloth electrodes, we presented two novel configurations (*i.e.*, laminated and tandem) for SCs, which were expected to increase the energy density and out-put voltage respectively.²²⁰ The fabric electrodes were prepared by dipping the non-woven cloth into a dispersion of carbon nanotubes and subsequent MnO_2 electrodeposition. In the lamination configuration (Fig. 21j), several pieces of MnO_2/CNT cloth were laminated in KOH aqueous electrolyte to construct individual electrodes that enable fold-increased areal capacitances and excellent cycling stability. Expectedly, the areal energy density increased with the laminations while the power density decreased, accounted for the increased resistance, as shown in Fig. 21k. In the tandem configuration, each unit supercapacitor was made of two pieces of MnO_2/CNT electrodes sandwiched with $\text{H}_3\text{PO}_4/\text{PVA}$ solid-state electrolyte. A high-output-voltage device could then be readily obtained by using a layer-by-layer assembly as displayed in Fig. 21l. The charge/discharge curves of the MnO_2/CNT -based SCs with different numbers of unit cells (Fig. 21m) suggested that this tandem stack structures precisely follow the principle of tandem capacitors.

Another kind of wearable supercapacitor is planar-shaped supercapacitor built on woven individual supercapacitor fibers or parallel arranged supercapacitor fibers. By using CNT coating on the common fibers (cellulose, metals and plastics etc.) or CNT yarns, robust and flexible electrodes were obtained. To enhance the capacity, pseudocapacitive materials such as the ZnO-MnO_2 nanorods arrays, ZnCo_2O_4 NWs and polyaniline NWs have elaborated on the fibers.²²²⁻²²⁶ Fiber-shaped supercapacitor can work independently or be woven into any shape desired. For example, Wang and co-workers present a simple design and fabrication method for a high-performance, thread-like supercapacitor, taking the form of a two-ply composite yarn consisting of two carbon nanotube (CNT) singles yarns that are infiltrated with polyaniline NW arrays.²²³ The CNT yarn possesses good mechanical properties, with tensile strength normally in the range $500\text{--}800 \text{ MPa}$. The optical microphotograph of the fiber supercapacitor by twisting two CNT@PANI single yarn with the PVA gel electrolyte is shown in Fig. 22a. Fig. 22b is an optical microphotograph of a model fabric composed of four conventional two-ply cotton yarns and four two-ply CNT@PANI@PVA yarn supercapacitors, giving a prototype of woven electronics. In Fig. 22c, the areal capacitance of CNT@PANI yarn-based supercapacitor and CNT yarn-based supercapacitor were compared, and a capacitance of 38 mF/cm^2 at the current density of 0.01 mA cm^{-2} was achieved by the former one. When evaluated under different bending conditions, the capacitance of the yarn supercapacitor changed very little (Fig. 22d). In the other hand, our group recently designed a flexible all-

solid-state planar integrated fiber supercapacitor based on hierarchical ZnCo_2O_4 nanowire arrays/carbon fiber electrodes (Fig. 22e).²²⁶ Fig. 22f depicts the measured specific capacitances of the flexible devices made of 2, 6, 10, 14, 20, and 30 composite fiber electrodes, presenting a significant rising trend with increasing fiber number. As shown by the equivalent circuit of the planar-integrated fiber supercapacitors (inset of Fig. 22f), this new structure exhibited an enhanced distributed-capacitance effect caused by the interaction among the non-adjacent opposite fiber electrodes, which can largely reduce the size of the device and achieve superior utilization efficiency and maximum functionality.

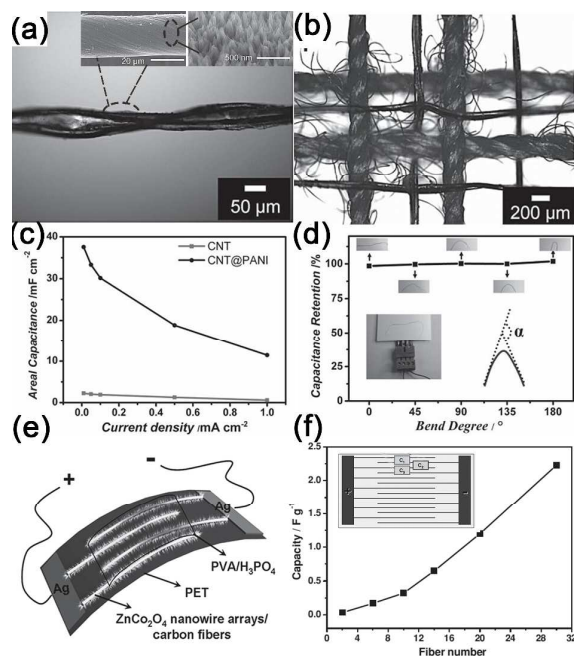


Fig. 22 (a) Two CNT@PANI@PVA single yarns twisted together to form a thread-like, two-ply yarn supercapacitor. Inset is the SEM images of CNT@PANI composite yarn. Ordered PANI NW arrays are on the surface of CNT yarn. (b) Yarn supercapacitors are co-woven with conventional cotton yarns to form a flexible electronic fabric with self-sufficient power source. (c) Areal capacitance plots of two-yarn capacitors. (d) Capacitance retention under different bending states. Reprinted with permission from ref. 223 © 2013, Wiley-VCH. (e) Schematic illustration of the configuration of the device. (f) The analysis of the equivalent circuit and enhanced distributed-capacitance effect for the flexible planar-integrated fiber supercapacitors. Reprinted with permission from ref. 226 © 2013, Wiley-VCH.

4.3 Dye-sensitized Solar cells

In 1991, the concept of using dye-sensitized colloidal TiO_2 nanoparticle films for photo-generated electrons was first proposed by Grätzel's group.²²⁷ It is a highly successful nanostructured solar cell that delivers energy conversion efficiency up to 15% till now.²²⁸⁻²³¹ Focusing on dye-sensitized solar cells (DSSC), we will review the most recent progress on NWs-based DSSCs. Compared with the traditional mesoporous TiO_2 nanoparticle networks, nanowires offer much shorter and faster electron transport path. Besides, NWs also scatter light and enhance light harvesting.²³² Moreover, In the flexible DSSCs, due to the robust structure for bendable stress release and unique functions through space adjustment, NWs have drawn enormous

attentions in the investigation of traditional flat flexible solar cells and fibrous ones wearable electronics.²³³

4.3.1 Flat flexible DSSCs

4.3.1.1 Photoanodes in flat flexible DSSCs

TiO₂ has been widely used as the photoanodes of DSSCs due to its suitable physical and chemical properties. Recently, some other semiconductor materials with the similar bandgap and properties to TiO₂ such as ZnO, SnO₂, Zn₂SnO₄, are also reported as the photoanodes.²³³⁻²³⁵ Transparent polymer substrates are efficient substrates for flexible DSSCs. However, the photovoltaic performance is hampered by the slow electron transport and large interface resistance caused by the low temperature sintering that ITO polymer substrates undergo. Recently, Jiang et al. demonstrated that NW based bendable electrode can release the bending stress effectively through space adjustment while the mesoporous network suffers the cracking or peeling, as shown in the schematic in Fig. 23a and b.²³³ ZnO-NW arrays grown on PET/ITO substrates showed no visible cracks or

signs of peeling off after bending (Fig. 23c and d). To overcome the low efficiency of NW-based DSSC caused by the lower surface area and lower dye-loading, ZnO nanoparticles were filled in the gaps between the nanowires. As expected, the modified DSSC combining both advantages exhibits higher efficiency and good flexibility (Fig. 23e). Later, Li et al. also developed a PVDF-nanofiber-reinforced TiO₂ electrode with high bendability.²³⁶ PVDF nanofibers could release the stress concentration in the electrode and minimize the occurrence of mechanical failure. After 500 or even 1000 cycles of bending tests for composite film based cells fabricated on ITO/PET, only a few cracks were visible, which is much robust than the PVDF-free TiO₂ cells. Moreover, PVDF polymers containing fluorine atoms, which have the smallest ionic radius and largest electronegativity, are expected to facilitate the ionic transport of electrolytes and reduce the recombination rate at the semiconductor/electrolyte interface. A remarkable efficiency of 4.78% was achieved. Therefore, NWs open a new way for the fabrication of flexible DSSCs.

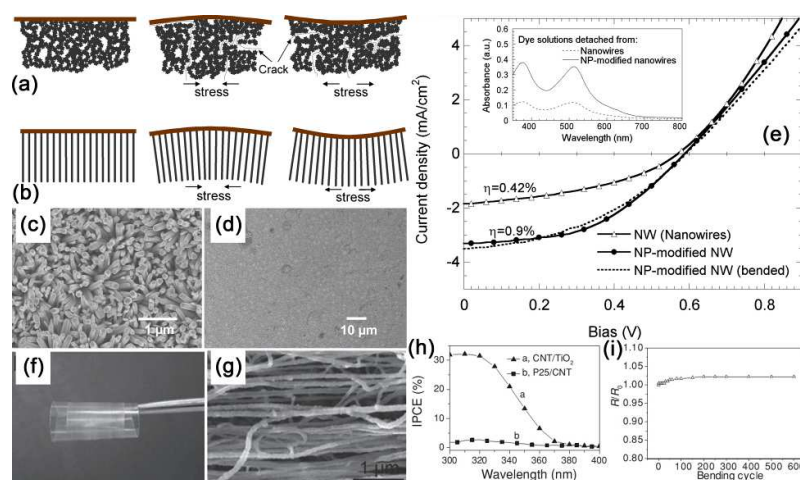


Fig. 23 Schematic shows of the bending stress release in nanocrystalline films of mesoporous network (a) and NW array (b). SEM images of the prepared ZnO NWs grown on flexible PET/ITO substrates by hydrothermal synthesis (c) and those after bending 2000 cycles with bending radius of 5 mm (d). (e) Current-voltage I-V characteristics of DSSCs constructed using ZnO NWs (triangle) and NP-modified ZnO NWs (circle), and the I-V curve (dashed) of the NP-modified ZnO-NW DSSC after bending to 5 mm radius for 5 cycles under illumination: 100 mW/cm², AM 1.5G. Inset: absorptions of dye solutions containing dyes from ZnO-NW film solid and NP-modified ZnO-NW film (dashed), respectively. Reprinted with permission from ref. 233 © 2008, AIP Publishing LLC. (f) Photograph of a CNT/TiO₂ film attached to a PET film. (g) High-resolution SEM image of the CNT/TiO₂ film, showing uniform oxide coatings around CNTs. (h) IPCE spectra of the CNT/TiO₂ film and the P25/CNT electrode. (i) Resistance change of a CNT/TiO₂ film on a PET film after the film was bent to a radius of 0.4 cm for different cycles. Reprinted with permission from ref. 239 © 2013, Wiley-VCH.

A transferred NW film on flexible polymer substrates provides another way to fabricate flexible DSSCs.²³⁷⁻²³⁹ The inverted process enables the thermal treatment of materials and prevents the thermal decomposition of the polymer substrates. An all-flexible DSSC was fabricated by assembling free-standing TiO₂ NW membrane with a Pt/Ti counter electrode and delivered an efficiency of 2.5%, which is comparable with the efficiency (3.8%) of rigid device constructed using similar materials.²³⁷ In another effort, Di et al reported a CNT/TiO₂ hybrid architecture for flexible photoelectrodes.²³⁹ As shown in Fig. 23f, the CNT/TiO₂ film can be transferred onto the PET film and exhibits good flexibility. In the photoanode, CNTs not only act as a scaffold, but also provide fast transport paths for photogenerated charges in the oxide. Without using additional transparent conducting oxide (TCO) substrates, this unique feature of the film boosts the incident photon-to-electron conversion efficiency to

32% in the UV light region without dye, outperforming TiO₂ nanoparticle electrodes fabricated on TCO substrates (Fig. 23h). Structure durability of the film was also tested by bending the film to a radius of 0.4 cm for hundreds of times. Only 2–3% increase in the resistance is observed after 600 bending cycles (Fig. 23i). Inverting transfer method allows for the high temperature annealing to enhancing the crystallinity.

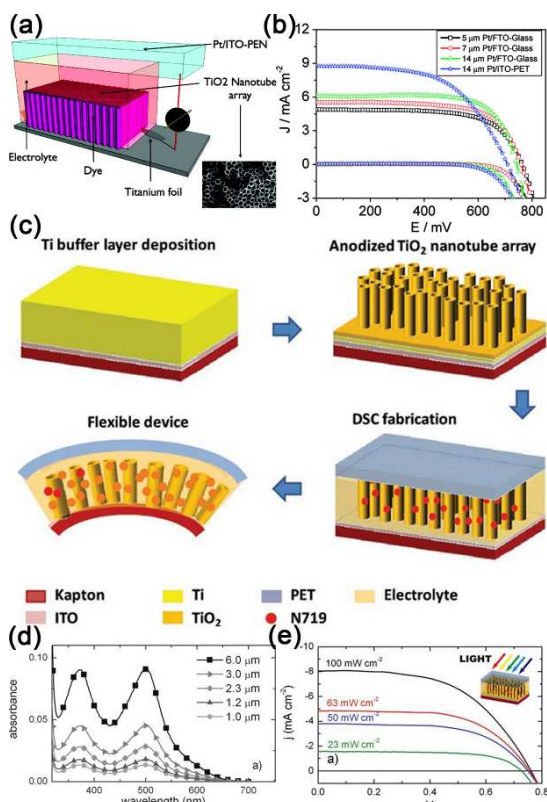


Fig. 24 (a) The schematic illustration of the flexible DSSC assembled with the TiO₂ nanotube arrays on Ti foil and Pt-coated PEN. (b) Current-voltage characteristic of solar cells based on different TiO₂ nanotube length using rigid (Pt/FTO-glass) and flexible (Pt/ITO-PEN) substrates. Solid lines were measured under AM 1.5 full sunlight (100mW/cm²) illumination. Dot lines were measured in the dark. Reprinted with permission from ref. 240 © 2008, American Chemical Society. (c) Schematic of fabrication of DSCs over flexible Kapton substrates. (d) UV-vis spectrum of N719 dye extracted from a series of TiO₂-nanotube arrays with different thicknesses. (e) J-V curves of a DSC under different simulated sunlight intensities. Back-irradiation geometry has been applied, as illustrated in the inset. Reprinted with permission from ref. 244 © 2011, Wiley-VCH.

Ti foil has been developed as both the precursor for TiO₂ NW arrays growth and substrates for subsequently DSSC fabrication. By facile anodization or hydrothermal process, highly ordered meso-structured TiO₂ nanotubes or NWs can be fabricated, in which superior photovoltaic performances can be achieved through the realization of photoanode materials with ordered structure.^{232,240-245} An excellent photoelectric conversion efficiency up to 8% has been achieved by the TiO₂ nanotube arrays coupled with the Pt-FTO glass counter electrode.²³¹ Recently, Kuang and co-workers reported a flexible DSSC using TiO₂ nanotube arrays on a Ti foil as the working electrode and Pt coated polyethylene naphthalate (ITO/PEN) as counterelectrode in combination with solvent-free ionic liquid electrolyte.²⁴⁰ TiO₂ nanotubes with the pore size of ~70 nm was fabricated (Fig. 24a). By varying the anodization time, the length of the NWs/nanotubes could be controlled to fit for best photoelectric conversion efficiency. The photocurrent-voltage curves are shown in Fig. 24b. Under AM 1.5 light irradiation from the back side, the flexible DSSC achieved an efficiency of 3.19%, which is comparable with that of the rigid DSSC assembled with Pt-FTO glass (3.3%). In order to obtain a flexible DSSC on the polymer

substrates, Galstyan et al. sputtered Ti on Kapton HN tape for electrochemical anodization, which enabled the post-treatment at 350 °C.²⁴⁴ The whole process of nanotube formation and cell fabrication is sketched in Fig. 24c. An almost-linear dependence of dye loading on the thickness of the nanotubes was experimentally found (Fig. 24d). A test cell based on a DSSC fabricated using the longest nanotube array (6 μm) was investigated under simulated sunlight irradiation in back-irradiation at AM 1.5G (100 mW cm⁻²) and mechanical filter to obtain light attenuation (Fig. 24e). Expectedly, a high efficiency of 3.5% was obtained at the light intensity of 63 mW/cm². Mesoporous TiO₂ nanotubes are promising for the prospective for the development of innovative technologies in the field of low-cost flexible photovoltaics.

4.3.1.2 Counter electrodes of flat flexible DSSCs

Pt is usually used as the catalytic materials for tri-iodide reduction and high conductivity. However, as a noble metal, Pt is expensive and exhibits instability in the methoxy propionitrile electrolyte solvents.²⁵⁰ Recently, several kinds of non-Pt materials have been exploited as the catalytic materials, such as carbon materials (activated carbon, graphene, carbon nanotubes etc.),^{251,252} conductive polymers (poly(3,4-ethylenedioxythiophene), PANI etc.),^{253, 254} inorganic materials (CoS, Co₉S₈ etc.²⁵⁵) and their compounds.²⁵⁶ 1D nanostructure based counter electrodes are one of the vital choices to prevent the fragmentation and detachment of the materials under tough bending conditions. For example, DSSC with CNT-based coatings on conductive glass exhibited photoelectric conversion efficiency of 10%, thanks to the high electrochemical catalytic activity, excellent conductivity and chemical stability.²⁵⁷ As a promising conductive material for transparent electrode, CNT can be used as the conductive cover to replace ITO or FTO underlying coating and Pt catalyst at the same time.²⁵⁸⁻²⁶⁰ The fabrication methods of CNT based flexible counter electrodes include the ink-coating process, growth-detachment-transfer process and directly usage of free-standing CNT films.²⁵⁹⁻²⁶² For instance, Chang et al. established a Pt nanoparticle (NP)/CNT hybrid counter electrode on Ti foil by using a stable dispersant consisting of poly(oxyethylene)diamine (POEM) segment and imide linkage functionalities.²⁶¹ The solution was coated on the foil by doctor blade technique, followed by annealing at 390°C to obtain the flexible electrode (Fig. 25a). Conversion efficiency of about 9.04% was obtained (Fig. 25b). The CNTs not only enhanced the surface area and Pt loading, but also served as the electrocatalyst. Recently, Malara et al. proposed a free-standing and ultrathin plate by compositing CNTs with polypropylene for the counter electrode,²⁵⁹ as shown in Fig. 25c. The extended etching treatment conditions dramatically benefit the electrochemical properties of the NC/electrolyte as well as the value of the series resistance of the plate (Fig. 25d). Flexible DSSC based on this plate gave a highest efficiency of 6.67%. In their later work, a much enhanced efficiency of 7.26% was obtained by transferring a vertically aligned carbon nanotube forest onto the CNT-polymer plates, demonstrating a promising implementation of the CNTs as an engineered flexible counter electrode.²⁶⁰

Metal oxides and sulphides were also used as counter electrodes of DSSCs.²⁶³⁻²⁶⁵ A maximum power conversion

efficiency of 7.67% was usually achieved for a cell with CoS nanorod arrays grown on the FTO-glass, which is nearly the same as that of a cell with a sputtered Pt counter electrode (7.70%).²⁶³ Lately, the authors fabricated the Co₉S₈ acicular nanorod arrays on a conducting plastic substrate by a two-step approach successfully.²⁶⁴ By chemical bath deposition, layered cobalt carbonate hydroxide acicular nanorod arrays (ANRAs) were fabricated on a conducting plastic substrate, followed by a simple ionic-exchange process in Na₂S solution to convert the precursor into Co₉S₈ nanorod arrays under facile conditions (Fig. 25e). In Fig. 25f, all the CV curves for the Co₉S₈ ANTAs-60 min, Co₉S₈ ANTAs-90 min, Co₉S₈ ANTAs-120 min, Co₉S₈ ANTAs-150 min and Co₉S₈ ANTAs-180 min CEs show two pairs of redox peaks, which reveal similar electrochemical behavior to that of the sputtered Pt CE. Finally, a power conversion efficiency of 5.47% was achieved, which was comparable to that of the DSSC using sputtered Pt (5.62%) on the same plastic substrates (Fig. 25g).

4.3.2 Fibrous DSSCs

Recently, there is a growing interest in making fiber-shaped photovoltaics owing to their promising applications in flexible electronics and wearable power supply.²⁶⁶ Compared with the flat DSSCs, thin fiber-shaped solar cells have the advantages of lightweight and wearability. Generally, optical fibers, carbon fibers or metal threads (Ti, stainless steel) are used as the fiber substrates. The basic structure of fiber-DSSCs consists of three

kinds of assembly, including the twisted, parallel arrangement by two wires or a single cable-like fiber wrapped by the functional layers, as shown in Fig. 26a.²⁶⁷⁻²⁷⁸

The twisted architecture is the mostly employed one among all fiber-DSSCs, in which one fiber is coated with the photoactive materials and the other one is counter electrode. The counter electrode (Pt wires, carbon fibers etc.) is twined on the working electrode with intervals to allow light absorption by dye molecules. Zou's group has devoted a lot of efforts on this kind of fiber DSSCs and achieved a high photo-electric conversion efficiency of 7% by using Pt wire as the counter electrode.^{132, 138} Peng's group reported a further enhanced result by utilizing anodized TiO₂ nanotube arrays on Ti thread as photoanode and Pt and Ni particle decorated CNT yarns as counter electrode.²⁷⁷ Fig. 26b display the schematic illustration and SEM image of the photovoltaic wire respectively. This fiber is quite strong, showing a tensile stress of hundreds MPa. Decorated by 18.64 wt% and 9.33 wt% of Pt and Ni nanoparticles respectively, a highest efficiency of 8.03% was obtained. Given the excellent performance, the twisted structure of fiber DSSCs is a promising candidate for practical application. Chen et al. constructed a series module by five twisted fiber DSSC, which can successfully drive three commercial light emitting diodes (LED) in parallel connection under illumination.²⁶⁹

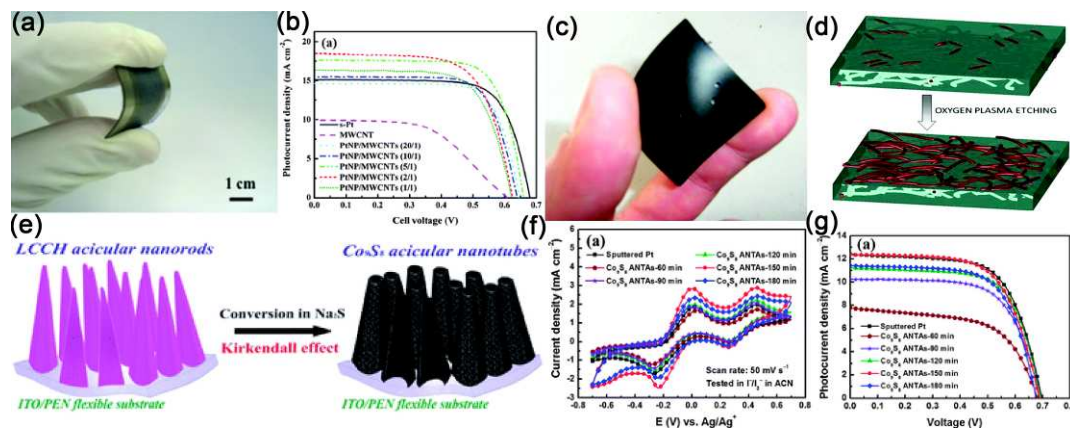


Fig. 25 (a) A picture of the flexible CE with Pt NP/MWCNT. (b) Photocurrent density–voltage curves of the DSSCs using Pt NP/MWCNT CEs with various ratios, measured at 100 mW/cm² light intensity. s-Pt was also used for comparison. Reprinted with permission from ref. 261 © 2012, The Royal Society of Chemistry. (c) A picture of a CNT-based monolithic counter electrodes and (d) a schematic representation of etching treatment effect. Reprinted with permission from ref. 259 © 2011, American Chemical Society. (e) Co₉S₈ acicular nanotube arrays (ANTAs) are prepared from LCCH acicular nanorod arrays (ANRAs) by soaking in Na₂S solution (0.01 M) for 3 h with the help of the Kirkendall effect. (f) CV curves for the sputtered Pt and the Co₉S₈ ANTAs CEs prepared with different periods of chemical bath deposition. (g) J–V curves of the DSSCs using sputtered Pt and Co₉S₈ ANTAs CEs prepared with different periods of CBD. Reprinted with permission from ref. 264 © 2013, The Royal Society of Chemistry.

Since the twisted structures usually lead to a large part of the working electrode being not covered by the Pt counter electrode and light wastage of the covered area, parallel arrangement was thus proposed.²⁶⁷ Wang et al. developed a novel methodology for the fabrication of an extended-area, flexible, transparent, double-sided, planar DSSC, formed with metal wire/ZnO-NW arrays as the working electrode and a Pt wire as the counter electrode. Highly ordered, single-crystalline, and high-density ZnO-NW arrays were uniformly deposited onto Fe microwires. The two metal wires were placed parallel to each other and encapsulated in a poly(ethylene terephthalate) (PET) or polydimethylsiloxane (PDMS) chamber containing the electrolyte (Fig. 26c). The double-wire DSSCs remain stable for a long period of time and

can be bent at large angles, up to 107°, reversibly, without any loss of performance.

Cable-like solar cells are also proposed by assembling the active materials on a single substrate wire layer by layer. Zhang et al. developed a cable-like DSSC based on a single Ti wire, by wrapping a carbon nanotube film around Ti wire-supported TiO₂ tube arrays as the transparent electrode (Fig. 26d).²⁷³ The CNT film ensures full contact with the underlying active layer, as well as uniform illumination along circumference through the entire DSSC. The single-wire DSSC shows a power conversion efficiency of 1.6% under standard illumination (AM 1.5, 100 mW/cm²). As the cable-like DSSC fiber is worked on back illumination with the bottom side unilluminated, Wang's group

integrated optical fibers and NW arrays as 3D cable-like DSSCs, shown in Fig. 26e.²⁷⁹ On the lower region of the fiber surface, dye-coated ZnO nanorod arrays are grown on the outer side of optical fibers, and then assembled with a Pt tube. The key principle is that the light entering from the axial direction inside the fiber experiences multiple internal reflections along the fiber and finally reaches to the dye molecules. When the DSSC is illuminated along the fiber axis, an efficiency of 0.44% is achieved, much better than the value (0.071%) obtained by a vertically illumination.

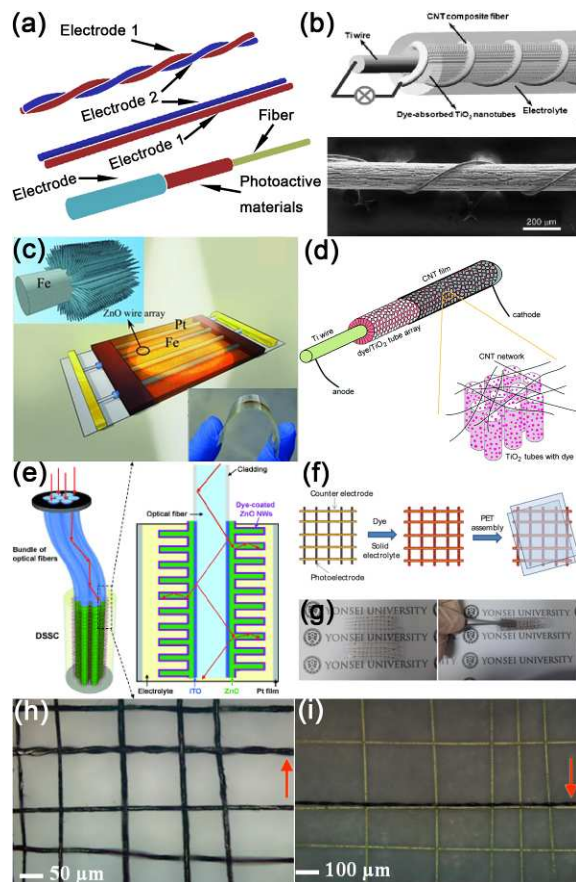


Fig. 26 (a) Schematic illustration of twisted, parallel and cable-like solar cells respectively. (b) Photovoltaic wire by twisting a TiO₂ nanotube-modified titanium wire which serves as a working electrode and an Fe₃O₄/CNT composite fiber which functions as the counter electrode together. Reprinted with permission from ref. 277 © 2013, Wiley-VCH. (c) Double-metal-wire/PET, double-sided, transparent DSSC device based on Pt-Fe microwires and ZnO NW-Fe microwires. Reprinted with permission from ref. 267 © 2012, Wiley-VCH. (d) Illustration of a coaxial single-wire structure DSSC, consisting of a core Ti wire, dye-grafted TiO₂ nanotube arrays, and a flexible, transparent CNT film wrapping around the wire. Reprinted with permission from ref. 273 © 2011, American Chemical Society. (e) Design and principle of a three-dimensional DSSC based on optic fiber. Reprinted with permission from ref. 279 © 2009, Wiley-VCH. (f) Procedure of all-solid, flexible solar textiles fabricated using DSSC with ZnO NR arrays on SS wires. (g) Photograph of a fabricated flexible woven solar cell. Reprinted with permission from ref. 272 © 2013, Elsevier B.V. (h) A fiber cell being woven with the other CNT fibers into a textile. (i) A fiber cell being woven into a textile composed of aramid fibers. Reprinted with permission from ref. 280 © 2012, American Chemical Society.

Based on the successful fabrication of fiber DSSCs, wearable DSSCs can be elaborated via a convenient weaving

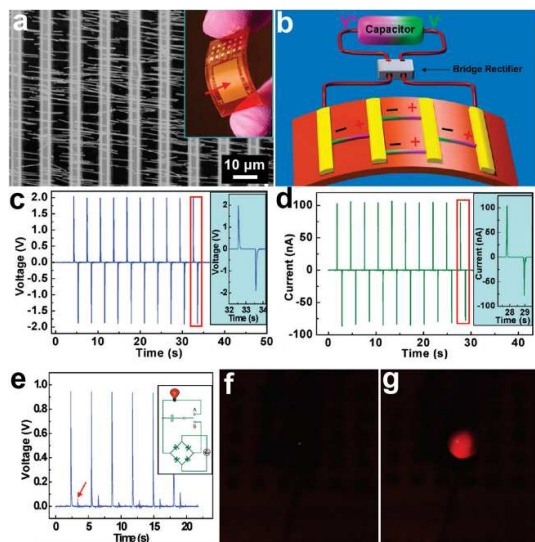
technology.^{272, 280} For instance, Chae et al. reported a woven DSSC by using ZnO nanorod vertically grown from fiber-type conductive stainless steel (SS) wires as photoanode and the Pt-coated SS wires as a counter electrode.²⁷² As shown in Fig. 26f, all solid, flexible solar textiles were fabricated by coating dyes and solid-state electrolyte, following with PET film package. The satin weaving structure was particularly employed due to larger illumination area compared to plain and twill weaving structures. The all-solid, flexible properties of solar textiles fabricated with ZnO NR-based DSSCs are shown in Fig. 26g. The solar textile with 10 × 10 wires exhibited an energy conversion efficiency of 2.57% with a short circuit current density of 20.2 mA/cm² at 100 mW/cm² illumination. Chen et al. also reported a woven DSSC by CNT fiber based solar cells.²⁸⁰ A twisted fiber DSSC consists of a CNT fiber and TiO₂ coated CNT fiber can be woven into CNT textiles and aramid textiles successfully (Fig. 26h and i), achieving an efficiency of 2.94%.

4.4 Generators

Since it was first proposed by Wang *et al.* in 2005, the self-powering nanotechnology has attracted much attention in energy harvesting area. This conception came into existence to serve the interests for driving portable electronics. With the rapid development and wide use of nanotechnology, it is the batteries rather than the devices that finally determine the total size and weight of the system. What's more, there is a pressing need to design a kind of rather small generator that could provide power for some micro/nano devices or medicine related devices, for example, implantable health monitors and artificial organs *etc.* So, to meet these technological challenges, it is highly necessary to develop the science and technology closely related to nanogenerator.

Wang and his co-workers demonstrated an approach to converting mechanical energy into electric power by using a vertical aligned piezoelectric (PZ) NWs²⁸¹ and accordingly, designed a series of nanogenerators with sufficient electric output. We provide here only one example, as it illustrates the basic principle and technology of nanogenerators.²⁸² In their experiments, vertically aligned ZnO NWs were transferred to a receiving substrate to form horizontally aligned arrays and then parallel-strips-like electrodes were deposited on the horizontal ZnO NW arrays. By connecting a bridge rectifier and a capacitor, a simple self-powered device which could harvest energy from the mechanical bending of the flexible substrate were successfully fabricated. Fig. 27a is the SEM image of ZnO NW arrays with deposited Au electrodes and the inset is the photograph of the as-fabricated nanogenerator. Orderly aligned ZnO NWs with diameter of ~200 nm served as the active material of the nanogenerators. By externally applied physical force, the flexible substrate was bended gradually, and correspondingly NWs happened to deform. The piezoelectric property of the ZnO NW brought a piezoelectric field along the length, which naturally caused a transient charge flow in the external circuit, as shown in Fig. 27b. Repeated bending and releasing of the substrate gives rise to an alternating flow of the charges in the external circuit. Time dependent open circuit voltages and short circuit currents are shown in Fig. 27c-d, respectively. From the figures we could see that an open-circuit voltage as high as 2.03 V and a peak output power density of ~11

mW/cm³ could be achieved from a single layer NW nanogenerator structure. As shown in inset of Fig. 27e, an integrated full wave rectifying bridge was connected with a red commercial LED to prove the successful fabrication of the high-
 5 output flexible nanogenerators. A total voltage source of 3.7 V and a maximum discharging current of 4.5 mA lead the lighting lasted 0.1-0.2 s of the LED, as shown in Fig. 27f-g. Through calculation, the effective energy generation efficiency is estimated to be ~4.6%. And by optimizing the density of the
 10 NWs on the substrate as well as the use multilayer integration, much more practical nanogenerators with high open-circuit voltages, high short circuit currents as well as much higher energy generation efficiency are bound to be created out.



15 **Fig. 27** (a) SEM image of active area of the nanogenerator. Inset is the photograph of an as-fabricated nanogenerator. (b) Demonstration of the operating principle of the nanogenerator when mechanical deformation is induced, where the “±” signs indicate the polarity of the local piezoelectric potential created in the NWs. (c-d) Open circuit voltage and short circuit current measurement of the nanogenerator. The measurement is performed at a strain of 0.1% and strain rate of 5% s⁻¹ under the frequency of 0.33 Hz. Insets are the enlarged view of the single cycle of signal. (e) Output voltage measured when connected with a full wave rectifying bridge. Where arrowhead points out that the signals of negative
 20 signs are reversed. Inset is the schematic of the charging-discharging circuit. (f-g) Image of the red LED before it was lit up and at the moment when it was lit up by the energy generated from the nanogenerator, respectively. Reprinted with permission from ref. 282 © 2010, American Chemical Society.

30 5 Integrated devices and systems

The successful fabrication of both NW-based flexible devices and energy conversion/storage sources offer numerous opportunities for the area of energy system, electronics, automobile, mechanical equipment et al. The integration of these
 35 semiconductor nanodevices, especially the passive devices with the power source devices would be of great interest in micro/nano systems' application. The design and fabrication of high-performance integrated nanopower-nanodevice system especially flexible system present several challenges, for example,
 40 impedance matching, electrical/mechanical stability and the improvement of operation efficiency *etc.* The challenges and limitations of these factors make corresponding improvement

hard. However, there are still a few works which focus on assembly of basic nanodevices into an integrated simple system
 45 that can work independently. In this section, methods and the ultimate performances of several integrated system will be briefly described.

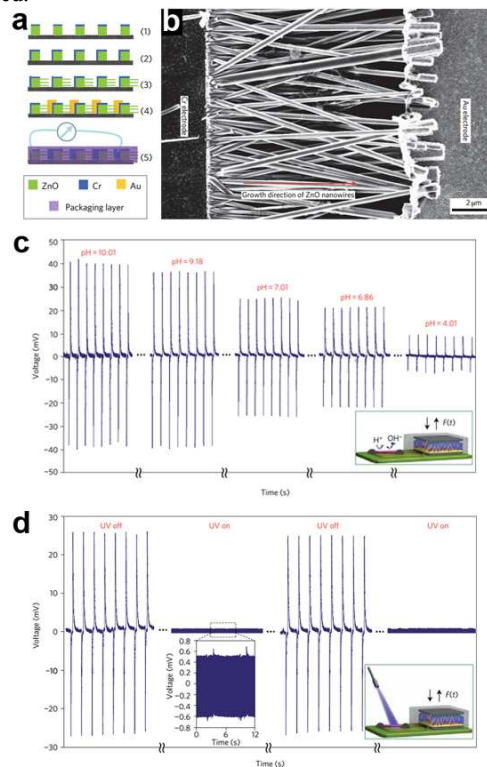


Fig. 28 (a) Schematic of the fabrication process of multiple lateral-NW-array integrated nanogenerator. (b) SEM images of a single row of the NWs bonded by metal electrodes. (c) Voltage drop across a single ZnO NW-based pH sensor powered by a VING with an output voltage of ~40 mV. (d) Voltage drop across a ZnO NW-based UV sensor powered by a VING with an output voltage of ~25mV. Insets are the schematics of the
 55 NW-based integrated systems. Reprinted with permission from ref. 283 © 2010, Macmillan Publisher Ltd.

Recently, Wang *et al.* proposed a flexible self-powered nanosystem, consisting of a multiple lateral-NW-array integrated nanogenerator (VING) and a NW based detector.²⁸³ The eventual
 60 aim of this design is self-driven, that is, realization the stable and persist operation of the passive devices without battery or external power source used. The key to provide high output voltage and power of the VING is the rational growth of the NWs during the VING fabrication procedure, as the voltage and power
 65 produced by a single NW are insufficient for a real device. Fig. 28a is the experimental procedures designed to fabricate the flexible VING. Briefly, rows of stripe-shaped ZnO pattern with a top and side layer of chromium was first achieved, then a wet chemical method was used to obtain horizontally grown ZnO NW
 70 arrays. Next, gold electrodes were deposited only on the above mentioned chromium layer side and at last a layer of soft polymer was spin-coated onto the device to improve the stability and mechanical robustness of the entire structure. Fig. 28b is the SEM image of a single-row VING structure, indicating the ordered
 75 alignment of the NWs and the good contacts between the NWs and the electrodes. The final flexible VING was made of 700 rows of NWs on a 125 μm Kapton film. In response to a low-

frequency mechanical strain of 0.19% at a straining rate of 2.13% s^{-1} , the average output voltage and the current pulse from the VING were measured to be ~ 1.2 V and ~ 26 nA respectively. To demonstrate the ‘self-powered’ performance, the VING was integrated with a single NW-based nanosensor. First a ZnO NW-based pH sensor was connected with the VING and the voltage across the nanosensor was monitored while changing the degree of acidity versus alkalinity in the target solution (Fig. 28c). An obvious and stable voltage variation corresponding to local pH change was observed, indicating the high sensitivity of the ‘self-powered’ pH meter. Then a ZnO NW-based UV sensor was also integrated with the VING. (Fig. 28d) When the UV light is turned off, the resistance of the ZnO NW is measured to be ~ 10 M Ω , which is comparable to the inner resistance of the VING. And voltage drop across the ZnO NW-based UV sensor was ~ 25 mV. Upon UV light illumination, the resistance of the ZnO NW dropped dramatically and the voltage drop across the ZnO NW-based UV sensor was very small. This clearly indicates that a VING with an output voltage of 20–40 mV can successfully power up various kinds of single-NW-based nanosensors.

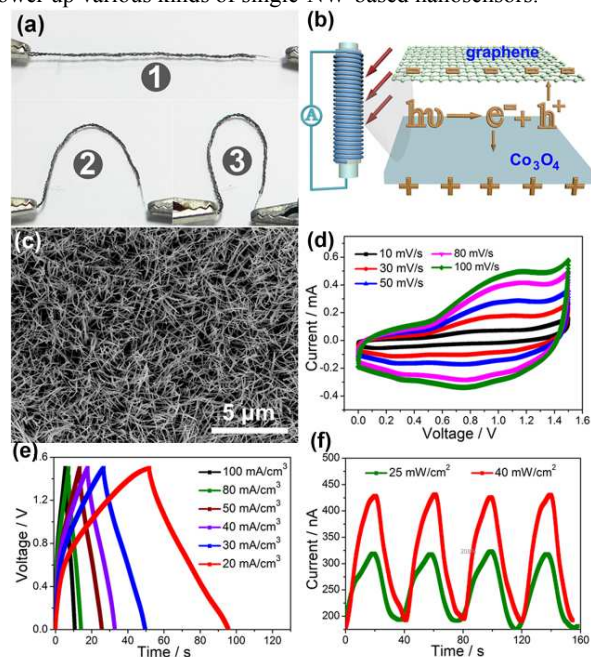


Fig. 29 (a-b) Photograph and schematic of the self-powered nanosystem powered by the Co₃O₄-graphene based fiber-shaped supercapacitor. 1-3 illustrate the different bending states of our flexible asymmetric supercapacitor. (c) SEM images of the as-synthesized Co₃O₄ NWs grown on nickel fiber used for supercapacitor. (d) CV curves, and (e) galvanostatic charge-discharge curves of the fiber-shaped supercapacitor. (f) Current response of the photodetector powered by the supercapacitor. Reprinted with permission from ref. 284 © 2014, WILEY-VCH.

Very recently, our group reported a self-powered photodetector, which was driven by a flexible fiber shaped supercapacitor (Fig. 29a-b).²⁸⁴ In this work, uniform Co₃O₄ NWs (Fig. 29c) was successfully synthesized on different type of metal fibers, namely nickel and titanium respectively, and then fabricated into two kinds of flexible all-solid-state supercapacitors. The as-synthesized Co₃O₄ NWs were proved to exhibit a high capacitance of 2.1 F cm⁻³ at current density of 20 mA cm⁻² and the final wire shaped all-solid-state supercapacitor was

demonstrated to have an impressive capacitive behaviour as well as high long cycling performances (showing in Fig. 29d-e). As discussed above, piezoelectric (PZ) ZnO NWs based nanogenerators could serve as the excellent energy-scavenging unit and could be integrated into a nanosystem to power electrical devices without the need of external batteries. By the same token, Co₃O₄ NWs based all-solid-state supercapacitors here could also act as the power sources. The as-prepared visible light photodetector made from carbon fibers/graphene, which also served as the negative electrode of the flexible all-solid-state asymmetric supercapacitor, was proved to have substantial response to white light irradiation (Fig. 29f). Our primary research work here indicate that the wire shaped flexible supercapacitors can efficiently be used to power electronic and optoelectronic devices, and if the material quality and the device structure could be continually improved, more complicated self-powered devices and systems with minimised sizes and promoted performances will come out. The harvesting of energy from ambient sources, energy storage/conversion and energy utilization will be more efficient.

6 Conclusions and outlooks

In this paper, the recent advances in design and fabrication of NW based flexible devices and their integration has been reviewed. We first present a brief description of different approaches to realize the synthesis of a versatile group of semiconductor NWs and a few methods for assembly of NWs array. Among the various semiconductors across an expansive area covering from metal oxides to III-V compound, II-VI compound and even multi metal compounds, many NWs and their combinations such as network, film as well as ordered arrays have significant promise for electronic, optoelectronic, photovoltaic, electrochemical and piezoelectric applications. Combining the unique geometry structure of NWs and the superior physical/chemical properties of semiconductors, many kind of typical nano/micro devices have been designed and fabricated out. We show that both individual NW and NW assembled structures offer high possible in the flexible device applications, for example flexible electrodes and transistors, flexible sensors, flexible display devices, flexible memories and logic gates, as well as flexible energy conversion and storage devices *et al.* However, for the NW synthesis and assembly, devices fabrication and system integration process that for economically viable applications, more significant research works will be required.

First, even the research in various NWs has been witnessed with fast development and substantial achievements, some issues such as the followings are still existed:

1. Lack good control over size of the NWs: The difference in properties caused by the size heterogeneity is very obvious. A more efficient synthesis method for more precise control of the NW's size is needed. Owing to the small dimensions and tendency to aggregate, manipulating NWs grown by bottom-up approaches is still challenging. There are two conceptually different types of approaches that can be used to address this problem. The first, a novel 3D printer can be invented to print quality NWs or uniform NW arrays directly. This scheme overcomes the inherent non-uniformity of NWs produced by

traditional bottom-up growth process while retaining the advantages of NWs itself. The second, improved top-down approaches are still attractive when integration and addressability are concerned. As for the manipulating of high density NW arrays, especially for addressability at the single NW level, a new kind of top-down approach has the advantage of being more amenable for large scale integration.

2. Difficulties in controlling the chemical or physical properties of the NWs. NWs with uniform size do not guarantee their uniformity in their properties such as electronic transport characteristics. To minimize the NW-to-NW variability is very important but still remains a challenge.

3. Combinations of different modifying methods over semiconductor NWs need to be systematically studied. Doping, surface modification, organic-inorganic hybrid, the formation of multiple compounds or heterojunctions *et al.* have been extensively studied for more than ten years. Still, a successful modification method would consider a numerous factors such as surface states, defects, traps, catalysts-induced contamination, orientation and polarization of the NWs. It seems a bit difficult to select an efficient way to modify the as-prepared NWs based on their ultimate use. So establishing an effective method for determining the modification process is quite critical.

4. The yield of NWs with high quality for scalable device fabrication and integration is far from enough.

5. Especially, each current NW assembly technique has its advantages and weakness and it appears some difficulties in printing NWs precisely on flexible substrates. The existing NW assembly techniques are also inefficient and have high cost of time. More appropriate NW assembly techniques need to be improved, and different types of assembly methods should be combined to give rise to high quality NW arrays.

Second, there is an obvious challenge in optimizing the configuration and fabrication process of the flexible devices. By taking the advantages of 1-D geometric features and excellent physical/chemical properties of NWs, a group of nanodevices have been created. However, most of them are just the basic unit which could only be used as the NWs' properties measurement.

In other words, most existed nanodevices are far functional enough to meet the need of practical work. For example, the NW based photodetectors are still at an early stage. Most current NW photodetectors have much lower performance in efficiency and bandwidth when compared with their classical counterparts,²⁸⁵

and the device-to-device variability of the performance has largely limited its development and application. Besides, measurement theory and methods about device properties should be found to the needs of specific and novel devices, for example, some sensors work in a harsh environment²⁸⁶ or under changing

conditions. New measurement and evaluation methods then should be brought up. Although optimization of the electronic/optoelectronic performance of many flexible devices is still under way, we view offering a few new, entry-level products as a new impetus for exploring this largely uncharted territory.

Roll-up portable displays, sensory skins and electronically steerable antenna arrays for wireless communication *et al.*, in our opinion, will be the satisfactory killer applications in the coming years. Furthermore, commercializing some of the important

applications will undoubtedly scare up more interest in this area.

60 Third, flexibility is one of the highlights of the devices and much more importance should be continuously attached to it. Flexible display device has been the fulfilment of an ever romantic dream. If an efficient way can be found to ensure both high performance and outstanding flexibility of the nanodevices, much more functional industrial products based on 1-D nanostructures will be designed.

At last, appropriate combinations of two or more as-fabricated NW devices will lead to some particularly exciting achievements. Combining appropriate electronic devices with energy units into a fully flexible system, in particular, is of special significance. Owing to the urgent demand of next-generation consumer electronics and with the rapid development of nanotechnology, integrated 1-D NW devices and systems are the most promising field to be realized in the near future. Besides, miniaturization, high integration and portability are the necessary requests of the future electronics. For example, nanoscale sensors can be equipped with tiny self-powered element and microwave communication components to serve as body-implantable sensing networks. Considering these, many startups want scientists to engage in applied research of fully flexible systems, rather than fundamental research of individual components. Fundamental breakthroughs, though important, should not dominate our research results list. The future of flexible inorganic NW electronics, in our opinion, will be largely dependent on how well we can balance the functionality, the stability as well as the cost issue of the NW-based flexible systems. We believe cooperation between entrepreneurs and scientists will certainly accelerate our research in this area. Assembling existing components into functional and smart systems, increasing their availability and reliability and then introducing them to the market, basically speaking, is the only way realizing commercial and industrial application of flexible electronics.

Acknowledgement

This work was supported by the National Natural Science Foundation (61377033 and 91123008).

Notes and references

^a State Key Laboratory for Superlattices and Microstructures, Institute of Semiconductor, Chinese Academy of Sciences, Beijing 100083, China. E-mail: gzshen@semi.ac.cn

^b School of Mathematics and Physics, University of Science and Technology Beijing, Beijing 100083, China.

† Z. Liu and J. Xu contribute equally to this work. They are visiting students from Huazhong University of Science and Technology.

- 1 B. K. Kim, S. -K. Lee, M. S. Kang, J. -H. Ahn and J. H. Cho, *ACS Nano*, 2012, **6**, 8646-8651.
- 2 D. Grimm, C. C. B. Bufon, C. Deneke, P. Atkinson, D. J. Thurmer, F. Schäffel, S. Gorantla, A. Bachmatiuk and O. G. Schmidt, *Nano Lett.*, 2013, **13**, 213-218.
- 3 L. Y. Yuan, J. J. Dai, X. H. Fan, T. Song, Y. T. Tao, K. Wang, Z. Xu, J. Zhang, X. D. Bai, P. X. Lu, J. Chen, J. Zhou and Z. L. Wang, *ACS Nano*, 2011, **5**, 4007-4013.
- 4 Y. Sun and J. A. Rogers, *Adv. Mater.*, 2007, **15**, 1897-1916.
- 5 R. T. Hamers, *Nature*, 2001, **412**, 489-490.

- 6 P.-C. Chen, G. Z. Shen, H. Chen, Y. G. Ha, C. Wu, S. Sukcharoenchoke, Y. Fu, J. Liu, A. Facchetti, T. J. Marks, M. E. Thompson and C. W. Zhou, *ACS Nano*, 2009, **3**, 3383-3390.
- 7 D. R. Cairns and G. P. Crawford, *Proc. IEEE*, 2005, **93**, 1451-1458.
- 8 J. Yoon, A. J. Baca, S. Park, P. Elvikis, J. B. Geddes, L. F. Li, R. H. Kim, J. L. Xiao, S. D. Wang, T. H. Kim, M. J. Motala, B. Y. Ahn, E. B. Duoss, J. A. Lewis, R. G. Nuzzo, P. M. Ferreira, Y. G. Huang, A. Rockett and J. A. Rogers, *Nat. Mater.*, 2008, **7**, 907-915.
- 9 C. Y. Chang, Y. J. Cheng, S. H. Hung, J. S. Wu, W. S. Kao, C. H. Lee and C. S. Hsu, *Adv. Mater.*, 2012, **24**, 549-553.
- 10 W. T. S. Huck, *Nat. Mater.*, 2005, **4**, 271-272.
- 11 K. Efimenko, M. Rackaitis, E. Manias, A. Vaziri, L. Mahadevan and J. Genzer, *Nat. Mater.*, 2005, **4**, 293-297.
- 12 S. Ju, A. Facchetti, Y. Xuan, J. Liu, F. Ishikawa, P. D. Ye, C. W. Zhou, T. J. Marks and D. B. Janes, *Nat. Nanotechnol.*, 2007, **2**, 378-384.
- 13 K. H. Cherenack, A. Z. Kattamis, B. Hekmatshoar, J. C. Sturm and S. Wagner, *IEEE Electron Device Lett.*, 2007, **28**, 1004-1006.
- 14 R. J. Hamers, *Nature*, 2001, **412**, 489-490.
- 15 S. R. Forrest, *Nature*, 2004, **428**, 911-918.
- 16 G. H. Gelinck, H. E. A. Huitema, E. V. Veenendaal, E. Cantatore, L. Schrijnemakers, J. B. P. H. V. D. Putten, T. C. T. Geuns, M. Beenhakkers, J. B. Giesbers, B. H. Huisman, E. J. Meijer, E. M. Benito, F. J. Touwslager, A. W. Marsman, B. J. E. V. Rens and D. M. Leeuw, *Nat. Mater.*, 2004, **3**, 106-110.
- 17 T. Someya, Y. Kato, T. Sekitani, S. Iba, Y. Noguchi, Y. Murase, H. Kawaguchi and T. Sakurai, *Proc. Natl. Acad. Sci. U. S. A.*, 2005, **102**, 12321-12325.
- 18 G. Eda, G. Fanchini and M. Chhowalla, *Nat. Nanotechnol.*, 2008, **3**, 270-274.
- 19 J. H. Burroughes, D. D. C. Bradley, A. R. Brown, R. N. Marks, K. Mackay, R. H. Friend, P. L. Burns and A. B. Holmes, *Nature*, 1990, **347**, 539-541.
- 20 S. Lamansky, P. Djurovich, D. Murphy, F. A. Razzaq, H. E. Lee, C. Adachi, P. E. Burrows, S. R. Forrest and M. E. Thompson, *J. Am. Chem. Soc.*, 2001, **123**, 4304-4312.
- 21 S. Reineke, F. Lindner, G. Schwartz, N. Seidler, K. Walzer, B. Lüssem and K. Leo, *Nature*, 2009, **459**, 234-238.
- 22 S. Soeren, D. V. Stijn, M. Kris, L. Martijin, G. Jan and H. Paul, *J. Appl. Phys.*, 2006, **99**, 114519(1-7).
- 23 R. Robert, M. Siddharth, O. Viorel, W. Robert, G. Michelle, D. Klaus, S. Oleg and D. Ananth, *Appl. Phys. Lett.*, 2006, **88**, 123502(1-3).
- 24 L. E. Kreno, K. Leong, O. K. Farha, M. Allendorf, R. P. V. Duyne and Joseph T. Hupp, *Chem. Rev.*, 2012, **112**, 1105-1125.
- 25 C. B. Black, B. Andrioletti, A. C. Try, C. Ruiperez and J. L. Sessler, *J. Am. Chem. Soc.*, 1999, **121**, 10438-10439.
- 26 J. Li, Y. J. Lu, Q. Ye, M. Cinke, J. Han and M. Meyyappan, *Nano Lett.*, 2003, **3**, 929-933.
- 27 A. Dodabalapur, L. Torsi and H. E. Katz, *Science*, 1995, **268**, 270.
- 28 K. Nomura, H. Ohta, K. Ueda, T. Kamiya, M. Hirano and H. Hosono, *Science*, 2003, **300**, 1269.
- 29 K. Nomura, H. Ohta, A. Takagi, T. Kamiya, M. Hirano and H. Hosono, *Nature*, 2004, **432**, 488.
- 30 Y. Yamashita, *Sci. Technol. Adv. Mat.*, 2009, **10**, 024313.
- 31 S. Y. Park, B. J. Kim, K. Kim, M. S. Kang, K. H. Lim, T. I. Lee, J. M. Myoung, H. K. Baik, J. H. Cho and Y. S. Kim, *Adv. Mater.*, 2012, **24**, 834.
- 32 N. A. Azarova, J. W. Owen, C. A. McLellan, M. A. Grimming, E. K. Chapman, J. E. Anthony and O. D. Jurchescu, *Org. Electron.*, 2010, **11**, 1960.
- 33 J. Li, C. Papadopoulos, J. M. Xu and M. Moskovits, *Appl. Phys. Lett.*, 1999, **75**, 367(1-3).
- 34 S. Cui, H. B. Liu, L. B. Gan, Y. L. Li and D. B. Zhu, *Adv. Mater.*, 2008, **20**, 2918-2925.
- 35 C. A. Wang, K. M. Ryu, A. Badmaev, J. L. Zhang and C. W. Zhou, *ACS Nano*, 2011, **5**, 1147.
- 36 C. Wang, A. Badmaev, A. Jooyaie, M. Q. Bao, K. L. Wang, K. Galatsis and C. W. Zhou, *ACS Nano*, 2011, **5**, 4169.
- 37 G. Z. Shen, B. Liang, X. F. Wang, P. C. Chen and C. W. Zhou, *ACS Nano*, 2011, **5**, 2155.
- 38 Z. Liu, H. T. Huang, B. Liang, X. F. Wang, Z. R. Wang, D. Chen and G. Z. Shen, *Opt. Express.*, 2012, **20**, 2982-2991.
- 39 D. M. Sun, M. Y. Timmermans, Y. Tian, A. G. Nasibulin, E. I. Kauppinen, S. Kishimoto, T. Mizutani and Y. Ohno, *Nat. Nanotechnol.*, 2011, **6**, 156-161.
- 40 C. Kocabas, H. S. Kim, T. Banks, J. A. Rogers, A. A. Pesetski, J. E. Baumgardner, S. V. Krishnaswamy and H. Zhang, *Proc. Natl. Acad. Sci. U. S. A.*, 2008, **105**, 1045-1049.
- 41 J. Appenzeller, *Proc. IEEE*, 2008, **96**, 201-211.
- 42 M. Rinkio, A. Johansson, G. S. Paraoanu and P. Törma, *Nano Lett.*, 2009, **9**, 643-647.
- 43 A. B. Kaul, E. W. Wong, L. Epp and B. D. Hunt, *Nano Lett.*, 2006, **6**, 952-947.
- 44 T. Durkop, S. A. Getty, E. Cobas and M. S. Fuhrer, *Nano Lett.*, 2004, **4**, 35-39.
- 45 E. T. Thostenson, Z. F. Ren and T. W. Chou, *Compos. Sci. Technol.*, 2001, **61**, 1899-1912.
- 46 T. Takenobu, T. Takahashi, T. Kanbara, K. Tsukagoshi, Y. Aoyagi and Y. Iwasa, *Appl. Phys. Lett.*, 2006, **88**, 33511-33513.
- 47 Q. Cao, S. H. Hur, Z. T. Zhu, Y. Sun, C. Wang, M. A. Meitl, M. Shim and J. A. Rogers, *Adv. Mater.*, 2006, **18**, 304-309.
- 48 E. Artukovic, M. Kaempgen, D. S. Hecht, S. Roth, and G. Gruner, *Nano Lett.*, 2005, **5**, 757-760.
- 49 F. N. Ishikawa, H. K. Chang, K. Ryu, P. C. Chen, A. Badmaev, L. G. D. Arco, G. Z. Shen and C. W. Zhou, *ACS Nano*, 2009, **3**, 73-79.
- 50 Y. Che, C. Wang, J. Liu, B. L. Liu, X. Lin, J. Parker, C. Beasley, H. S. P. Wong and C. W. Zhou, *ACS Nano*, 2012, **6**, 7454-7462.
- 51 E. Stern, J. F. Klemic, D. A. Routenberg, P. N. Wyrembak, D. B. T. Evans, A. D. Hamilton, D. A. Lavan, T. M. Fahmy and M. A. Reed, *Nature*, 2007, **445**, 519-522.
- 52 Z. Liu, B. Liang, G. Chen, G. Yu, Z. Xie, L. N. Gao, D. Chen and G. Z. Shen, *J. Mater. Chem. C*, 2013, **1**, 131-137.
- 53 G. D. Mahan, R. Gupta, Q. Xiong, C. K. Adu, and P. C. Eklund, *Phys. Rev. B*, 2003, **68**, 073402(1-4).
- 54 M. S. Gudiksen, L. J. Lauhon, J. F. Wang, D. C. Smith and C. M. Lieber, *Nature*, 2002, **415**, 617-620.
- 55 R. Q. Zhang, Y. Lifshitz and S. T. Lee, *Adv. Mater.*, 2003, **15**, 635-640.
- 56 Z. Liu, G. Chen, B. Liang, G. Yu, H. T. Huang, D. Chen and G. Z. Shen, *Opt. Express.*, 2013, **21**, 7799-7810.
- 57 A. I. Hochbaum and P. D. Yang, *Chem. Rev.*, 2010, **110**, 527-546.
- 58 P. D. Yang, R. X. Yan and M. Fardy, *Nano Lett.*, 2010, **10**, 1529-1536.
- 59 H. T. Huang, B. Liang, Z. Liu, X. F. Wang, D. Chen and G. Z. Shen, *J. Mater. Chem.*, 2012, **22**, 13428-13445.
- 60 M. Law, J. Goldberger and P. D. Yang, *Annu. Rev. Mater. Res.*, 2004, **34**, 83-122.
- 61 B. M. Wen, J. E. Sader and J. J. Boland, *Phys. Rev. Lett.*, 2008, **101**, 175502(1-4).
- 62 D.-H. Kim, N. S. Lu, R. Ghaffari and J. A. Rogers, *NPG Asia Mater.*, 2012, **4**, 15(1-9).
- 63 X. F. Wang, B. Liu, Q. F. Wang, W. F. Song, X. J. Hou, D. Chen, Y.-B. Chen and G. Z. Shen, *Adv. Mater.*, 2013, **25**, 1479-1486.
- 64 B. Liu, X. F. Wang, H. T. Chen, Z. R. Wang, D. Chen, Y.-B. Cheng, C. W. Zhou and G. Z. Shen, *Sci. Rep.*, 2013, **3**.
- 65 X. Wang, J. Zhuang, Q. Peng and Y. D. Li, *Nature*, 2005, **437**, 121-124.
- 66 Y. Cui, L. J. Lauhon, M. S. Gudiksen, J. F. Wang and C. M. Lieber, *Appl. Phys. Lett.* 2001, **78**, 2214(1-3).
- 67 C. Wang, Y. J. Hu, C. M. Lieber and S. S. Heng, *J. Am. Chem. Soc.*, 2008, **130**, 8902-8903.
- 68 J. M. Cai, P. Ruffieux, R. Jaafar, M. Bieri, T. Braun, S. Blankenburg, M. Muoth, A. P. Seitsonen, M. Saleh, X. L. Feng, K. Müllen and R. Fasel, *Nature*, 2010, **466**, 470-473.
- 69 G. B. Rossi, G. Beaucage, T. D. Dang and R. A. Vaia, *Nano Lett.*, 2002, **2**, 319-323.
- 70 J. D. Holmes, K. P. Johnston, R. C. Doty and B. A. Korgel, *Science*, 2000, **287**, 1471-1473.
- 71 Y. G. Sun, B. Gates, B. Mayer and Y. N. Xia, *Nano Lett.*, 2002, **2**, 165-168.
- 72 B. Weintraub, Z. Z. Zhou, Y. H. Li and Y. L. Deng, *Nanoscale*, 2010, **2**, 1573-1587.

- 73 A. P. Alivisatos, *J. Phys. Chem.*, **1996**, *100*, 13226-13239.
- 74 J. Xu, Y. G. Zhu, H. T. Huang, Z. Xie, D. Chen and G. Z. Shen, *CrystEngComm*, 2011, **13**, 2629-2635.
- 75 A. Birkel, N. Loges, E. Mugnaioli, R. Branscheid, D. Koll, S. Frank, M. Panthöfer and W. Tremel, *Langmuir*, 2010, **26**, 3590-3595.
- 76 X. M. Sun and Y. D. Li, *Adv. Mater.*, 2005, **17**, 2626-2630.
- 77 Z. P. Zhu, Y. Yang, J. B. Liang, Z. K. Hu, S. Li, S. Peng and Y. T. Qian, *J. Phys. Chem. B*, 2003, **107**, 12658-12661.
- 78 T. Y. Zhai, X. S. Fang, M. Y. Liao, X. J. Liu, H. B. Zeng, B. Yoshio and D. Golberg, *Sensors*, 2009, **9**, 6504-6529.
- 79 G. Z. Shen, J. Xu, X. F. Wang, H. T. Huang and D. Chen, *Adv. Mater.*, 2011, **23**, 771.
- 80 G. Chen, Z. Liu, B. Liang, G. Yu, Z. Xie, H. T. Huang, B. Liu, X. F. Wang, D. Chen and G. Z. Shen, *Adv. Func. Mater.*, 2013, **21**, 2681.
- 81 D. Routkevitch, T. Bibioni, M. Moskovits and J. M. Xu, *J. Phys. Chem.*, 1996, **100**, 14037-14047.
- 82 L. L. Wang, J. N. Deng, Z. Lou, and T. Zhang, *J. Mater. Chem. A*, 2014, **2**, 10022-10028.
- 83 L. Y. Zhang, J. Feng and D. S. Xue, *Mater. Lett.*, 2007, **61**, 1363.
- 84 D. S. Xue, L. Y. Zhang, A. B. Gui and X. F. Xu, *Appl. Phys. A*, 2005, **80**, 439.
- 85 S. M. Roper, H. S. Davis, S. A. Norris, A. A. Golovin, P. W. Voorhees and M. Weiss, *J. Appl. Phys.* 2007, **102**, 034304(1-7).
- 86 K. C. Grabar, R. G. Freeman, M. B. Hommer, and M. J. Natan, *Anal. Chem.* 1995, **67**, 735-743.
- 87 R. S. Wagner, W. C. Ellis, K. A. Jackson, and S. M. Arnold, *J. Appl. Phys.*, 1964, **35**, 2993(1-8).
- 88 Y. Y. Wu and P. D. Yang, *J. Am. Chem. Soc.*, 2001, **123**, 3165-3166.
- 89 K. -K. Lew, L. Pan, E. C. Dickey and J. M. Redwing, *Adv. Mater.*, 2003, **15**, 2073-2076.
- 90 Y. Ding, P. X. Gao, and Z. L. Wang, *J. Am. Chem. Soc.*, 2004, **126**, 2066-2072.
- 91 Y. Li, Y. Bando and D. Golberg, *Adv. Mater.*, 2003, **15**, 581-585.
- 92 Q. Wan, M. Wei, D. Zhi, J. L. MacManus-Driscoll and M. G. Blamire, *Adv. Mater.*, 2006, **18**, 234.
- 93 Q. Wan, P. Feng and T. H. Wang, *Appl. Phys. Lett.*, 2006, **89**, 123102.
- 94 J. H. He, J. H. Hsu, C. W. Wang, H. N. Lin, L. J. Chen and Z. L. Wang, *J. Phys. Chem. B*, 2006, **110**, 50-53.
- 95 L. E. Greene, M. Law, D. H. Tan, M. Montano, J. Goldberger, G. Somorjai and P. D. Yang, *Nano Lett.*, 2005, **5**, 1231-1236.
- 96 Z. Ying, Q. Wan, Z. T. Song and S. L. Feng, *Mater. Lett.* 2005, **59**, 1670-1672.
- 97 N. Sköld, L. S. Karlsson, M. W. Larsson, M. -E. Pistol, W. Seifert, J. Trägårdh and L. Samuelson, *Nano Lett.*, 2005, **5**, 1943-1947.
- 98 A. Umar, S. H. Kim, Y. -S. Lee, K. S. Nahm and Y. B. Hahn, *J. Cryst. Growth*, 2005, **282**, 131-136.
- 99 S. H. Sun, G. W. Meng, Y. W. Wang, T. Gao, M. G. Zhang, Y. T. Tian, X. S. Peng and L. D. Zhang, *Appl. Phys. A*, 2003, **76**, 287-289.
- 100 X. S. Peng, G. W. Meng, J. Zhang, X. F. Wang, Y. W. Wang, C. Z. Wang and L. D. Zhang, *J. Mater. Chem.*, 2002, **12**, 1602-1605.
- 101 D. H. Fan, *J. Cryst. Growth*, 2009, **311**, 2300-2304.
- 102 L. S. Wang, X. Z. Zhang, S. Q. Zhao, G. Y. Zhou, Y. L. Zhou and J. J. Qi, *Appl. Phys. Lett.* 2005, **86**, 024108(1-3).
- 103 Y. Huang, X. F. Duan, Q. Q. Wei and C. M. Lieber, *Science*, 2001, **291**, 630-633.
- 104 G. H. Yu, A. Y. Cao and C. M. Lieber, *Nat. Nanotechnol.*, 2007, **2**, 372-377.
- 105 C. M. Hangarter and N. V. Myung, *Chem. Mater.*, 2005, **17**, 1320-1324.
- 106 E. M. Freer, O. Grachev, X. F. Duan, S. Martin and D. P. Stumbo, *Nat. Nanotechnol.*, 2010, **5**, 525-530.
- 107 Z. Y. Fan, J. C. Ho, Z. A. Jacobson, R. Yerushalmi, R. L. Alley, H. Razavi and A. Javey, *Nano Lett.*, 2008, **8**, 20-25.
- 108 A. C. Ford, J. C. Ho, Z. Y. Fan, O. Ergen, V. Altoe, S. Aloni, H. Razavi and A. Javey, *Nano Res.*, 2008, **1**, 32-39.
- 109 R. Yerushalmi, Z. A. Jacobson, J. C. Ho, Z. Y. Fan and A. Javey, *Appl. Phys. Lett.*, 2007, **91**, 203104(1-3).
- 110 S.-Y. Min, T.-S. Kim, B.-J. Kim, H. Cho, Y.-Y. Noh, H. Yang, J. H. Cho and T.-W. Lee, *Nat. Commun.*, 2013, **4**, 1773(1-9).
- 111 H. Cho, S.-Y. Min, and T.-W. Lee, *Macromol. Mater. Eng.*, 2013, **298**, 475-486.
- 112 D. Li, and Y. Xia, *Adv. Mater.*, 2004, **16**, 1151-1170.
- 113 A. L. Briseno, s. c. b. Mannsfeld, S. A. Jenekhe, Z. N. Bao and Y. N. Xia, *Mater. Today*, 2008, **11**, 38-47.
- 114 N. L. Liu, Y. Zhou, N. Ai, C. Luo, J. B. Peng, J. Wang, J. Pei and Y. Cao, *Langmuir*, 2011, **27**, 14710-14715.
- 115 X. J. Zhang, J. S. Jie, W. F. Zhang, C. Y. Zhang, L. B. Luo, Z. B. He, X. H. Zhang, W. J. Zhang, C. Lee and S. T. Lee, *Adv. Mater.*, 2008, **20**, 2427-2432.
- 116 Y. P. Zhang, X. D. Wang, Y. M. Wu, J. S. Jie, X. W. Zhang, Y. L. Xing, H. H. Wu, B. Zou, X. J. Zhang and X. H. Zhang, *J. Mater. Chem.*, 2012, **22**, 14357-14362.
- 117 L. Persano, C. Degdeviren, Y. W. Su, Y. H. Zhang, S. Girardo, D. Pisignano, Y. G. Huang and J. A. Rogers, *Nat. Commun.*, 2013, **4**, 1633(1-10).
- 118 A. R. Madaria, A. Kumar, F. N. Ishikawa and C. W. Zhou, *Nano Res.* 2010, **3**, 564-573.
- 119 L. B. Hu, H. S. Kim, J. -Y. Lee, P. Peumans and Y. Cui, *ACS Nano*, 2010, **5**, 2955-2963.
- 120 A. R. Rathmell and B. J. Wiley, *Adv. Mater.*, 2011, **23**, 4798-4803.
- 121 T. Takahashi, K. Takei, E. Adabi, Z. Y. Fan, A. M. Niknejad and A. Javey, *ACS Nano*, 2010, **10**, 5855-5860.
- 122 M. C. McAlpine, H. Ahmad, D. W. Wang and J. R. Heath, *Nature Mater.*, 2007, **6**, 379-384.
- 123 D. K. Kim, Y. M. Lai, T. R. Vemulkar, and C. R. Kagan, *ACS Nano*, 2011, **12**, 10074-10083.
- 124 D. V. Talapin and C. B. Murray, *Science*, 2005, **310**, 86-89.
- 125 F. Patolsky and C. M. Lieber, *Mater. Today*, 2005, **8**, 20-28.
- 126 H. Kind, H. Q. Yan, B. Messer, M. Law, and P. D. Yang, *Adv. Mater.* 2002, **14**, 158-160.
- 127 C.-H. Lin, T.-T. Chen, and Y.-F. Chen, *Opt. Express*, 2008, **16**, 16916-16922.
- 128 D. Zhang, C. Li, S. Han, X. Liu, T. Tang, W. Jin, and C. W. Zhou, *A Mater. Sci. Process.* 2003, **77**, 163-166.
- 129 L. Wang, M. Lu, P. Lv, J. S. Jie, T. X. Yan, Y. Q. Yu, C. Y. Wu, Y. Zhang, C. Xie, P. Jiang, Z. Wang and Z. H. Hu, *Sci. Adv. Mater.*, 2012, **4**, 332-336.
- 130 T. Y. Zhai, M. F. Ye, L. Li, X. S. Fang, M. Y. Liao, Y. F. Li, Y. Koide, Y. Bando and D. Golberg, *Adv. Mater.*, 2010, **22**, 4530-4533.
- 131 Z. T. You, X. S. Fang, M. Y. Liao, X. J. Xu, L. Li, B. D. Liu, Y. Koide, Y. Ma, J. N. Yao, Y. Bando and D. Golberg, *ACS Nano*, 2010, **4**, 1596-1602.
- 132 Z. X. Wang, M. Safdar, C. Jiang and J. He, *Nano Lett.*, 2012, **12**, 4715-4721.
- 133 J. Svensson, N. Anttu, N. Vainorius, B. M. Borg and L. E. Wernersson, *Nano Lett.*, 2013, **13**, 1380-1385.
- 134 C. Y. Yan, N. D. Singh, and P. S. Lee, *Appl. Phys. Lett.* 2010, **96**, 053108.
- 135 C. Y. Yan and P. S. Lee, *Sci. Adv. Mater.* 2012, **4**, 241-253.
- 136 S. Bai, W. W. Wu, Y. Qin, N. Y. Cui, D. J. Bayerl and X. D. Wang, *Adv. Funct. Mater.*, 2011, **21**, 4464-4469.
- 137 G. Chen, Z. Liu, B. Liang, G. Yu, Z. Xie, H. T. Huang, B. Liu, X. F. Wang, D. Chen, M. Q. Zhu, and G. Z. Shen, *Adv. Funct. Mater.* 2013, **23**, 2681-2690.
- 138 R. R. He and P. D. Yang, *Nat. Nanotechnol.*, 2006, **1**, 42-46.
- 139 J. Zhou, Y. D. Gu, P. Fei, W. J. Mai, Y. F. Gao, R. S. Yang, G. Bao and Z. L. Wang, *Nano Lett.*, 2008, **8**, 3035-3034.
- 140 S. C. B. Mannsfeld, B. C-K. Tee, C-K. Tee, R. M. Stoltenberg, C. V. H-H. Chen, S. Barman, B. V. O. Muir, A. N. Sokolov, C. Reese and Z. N. Bao, *Nat. Mater.*, 2010, **9**, 859-864.
- 141 K. Takei, T. Takahashi, J. C. Ho, H. Ko, A. G. Gillies, P. W. Leu, R. S. Fearing and A. Javey, *Nat. Mater.*, 2010, **9**, 821-826.
- 142 C. Wang, D. Hwang, Z. B. Zhu, K. Takei, J. Park, T. Chen, B. W. Ma and A. Javey, *Nat. Mater.*, 2013, **12**, 899-904.
- 143 M. C. McAlpine, R. S. Friedman, S. Jin, K-H. Lin, W. U. Wang and C. M. Lieber, *Nano Lett.*, 2003, **3**, 1531-1535.
- 144 A. Nadarajah, R. C. Word, J. Meiss, and R. Köhnenkamp, *Nano Lett.*, 2008, **8**, 534-537.
- 145 A. Javey, S. W. Nam, R. S. Friedman, H. Yan and C. M. Lieber, *Nano Lett.*, 2007, **7**, 773-777.

- 146 Y. G. Sun, H-S. Kim, E. Menard, S. Kim, I. Adesida and J. A. Rogers, *small*, 2006, 2, 11, 1330-1334.
- 147 Q. Cao, H-S. Kim, N. Pimparkar, J. P. Kulkarni, C. Wang, M. Shim, K. Roy, M. A. Alam and J. A. Rogers, *Nature*, 2008, **454**, 495-500.
- 5 148 M. Armand and J. M. Tarascon, *Nature*, 2008, **451**, 652-657.
- 149 H. Wu and Y. Cui, *Nano Today*, 2012, 7, 414-429.
- 150 A. S. Arico, P. Bruce, B. Scrosati, J.-M. Tarascon and W. van Schalkwijk, *Nat Mater.*, 2005, **4**, 366-377.
- 151 S. Iijima, *Nature*, 1991, **354**, 56-58.
- 10 152 B. Gao, C. Bower, J. D. Lorentzen, L. Fleming, A. Kleinhammes, X. P. Tang, L. E. McNeil, Y. Wu and O. Zhou, *Chemical Physics Letters*, 2000, **327**, 69-75.
- 153 S. W. Lee, N. Yabuuchi, B. M. Gallant, S. Chen, B.-S. Kim, P. T. Hammond and Y. Shao-Horn, *Nat Nano*, 2010, **5**, 531-537.
- 15 154 S. Y. Chew, S. H. Ng, J. Wang, P. Novák, F. Krumeich, S. L. Chou, J. Chen and H. K. Liu, *Carbon*, 2009, **47**, 2976-2983.
- 155 J. Chen, A. I. Minett, Y. Liu, C. Lynam, P. Sherrell, C. Wang and G. G. Wallace, *Adv. Mater.*, 2008, **20**, 566-570.
- 156 B. J. Landi, M. J. Ganter, C. M. Schauerma, C. D. Cress and R. P. Raffaele, *J. Mater. Chem.*, 2008, **112**, 7509-7515.
- 20 157 X. Li, J. Yang, Y. Hu, J. Wang, Y. Li, M. Cai, R. Li and X. Sun, *J. Mater. Chem.*, 2012, **22**, 18847-18853.
- 158 L. Hu, H. Wu, F. La Mantia, Y. Yang and Y. Cui, *ACS Nano*, 2010, **4**, 5843-5848.
- 25 159 K. Wang, S. Luo, Y. Wu, X. F. He, F. Zhao, J. P. Wang, K. L. Jiang and S. S. Fan, *Adv. Funct. Mater.*, 2013, **23**, 846-853.
- 160 L. Hu, F. La Mantia, H. Wu, X. Xie, J. McDonough, M. Pasta and Y. Cui, *Adv. Energy Mater.*, 2011, **1**, 1012-1017.
- 161 V. L. Pushparaj, M. M. Shaijumon, A. Kumar, S. Murugesan, L. Ci, R. Vajtai, R. J. Linhardt, O. Nalamasu and P. M. Ajayan, *Proc. Natl. Acad. Sci. U. S. A.*, 2007, **104**, 13574-13577.
- 30 162 L. Hu and Y. Cui, *Energy Environ. Sci.*, 2012, **5**, 6423-6435.
- 163 L. Hu, J. W. Choi, Y. Yang, S. Jeong, F. La Mantia, L.-F. Cui and Y. Cui, *Proc. Natl. Acad. Sci. U. S. A.*, 2009, **106**, 21490-21494.
- 35 164 B. Liu, X. Wang, H. Chen, Z. Wang, ChenDi, Y.-B. Cheng, C. Zhou and G. Shen, *Sci. Rep.*, 2013, **3**.
- 165 C. K. Chan, X. F. Zhang and Y. Cui, *Nano Lett.*, 2007, **8**, 307-309.
- 166 M. Tian, W. Wang, S.-H. Lee, Y.-C. Lee and R. Yang, *J. Power Sources*, 2011, **196**, 10207-10212.
- 40 167 B. Liu, J. Zhang, X. Wang, G. Chen, D. Chen, C. Zhou and G. Shen, *Nano Lett.*, 2012, **12**, 3005-3011.
- 168 L. Wang, B. Liu, S. Ran, H. Huang, X. Wang, B. Liang, D. Chen and G. Shen, *J. Mater. Chem.*, 2012, **22**, 23541-23546.
- 169 L. Gao, X. Wang, Z. Xie, W. Song, L. Wang, X. Wu, F. Qu, D. Chen and G. Shen, *J. Mater. Chem. A*, 2013, **1**, 7167-7173.
- 45 170 W. Li, X. Wang, B. Liu, S. Luo, Z. Liu, X. Hou, Q. Xiang, D. Chen and G. Shen, *Chem. Eur. J.*, 2013, **19**, 8650-8656.
- 171 W. Li, X. Wang, B. Liu, J. Xu, B. Liang, T. Luo, S. Luo, D. Chen and G. Shen, *Nanoscale*, 2013, **5**, 10291-10299.
- 50 172 B. Liu, X. Wang, B. Liu, Q. Wang, D. Tan, W. Song, X. Hou, D. Chen and G. Shen, *Nano Res.*, 2013, **6**, 525-534.
- 173 X. Wang, Q. Xiang, B. Liu, L. Wang, T. Luo, D. Chen and G. Shen, *Sci. Rep.*, 2013, **3**.
- 174 J.-Y. Choi, D. J. Lee, Y. M. Lee, Y.-G. Lee, K. M. Kim, J.-K. Park and K. Y. Cho, *Adv. Funct. Mater.*, 2013, **23**, 2108-2114.
- 55 175 Y. Cui and C. M. Lieber, *Science*, 2001, **291**, 851-853.
- 176 C. K. Chan, H. Peng, G. Liu, K. McIlwrath, X. F. Zhang, R. A. Huggins and Y. Cui, *Nat. Nanotechnol.*, 2008, **3**, 31-35.
- 177 S. Liu, Z. Wang, C. Yu, H. B. Wu, G. Wang, Q. Dong, J. Qiu, A. Eychmüller and X. W. Lou, *Adv. Mater.*, 2013, **25**, 3462-3467.
- 60 178 W. W. Li, X. F. Wang, B. Liu, S. J. Luo, Z. Liu, X. J. Hou, Q. Y. Xiang, D. Chen and G. Z. Shen, *Chem. Eur. J.*, 2013, **19**, 8650-8656.
- 179 L. Lin, Z. Wu, S. Yuan and X. B. Zhang, *Energy Environ. Sci.*, 2014, **7**, 2101-2122.
- 65 180 G. Zhou, F. Li and H. M. Cheng, *Energy Environ. Sci.*, 2014, **7**, 1307-1338.
- 181 H. Gwon, J. Hong, H. Kim, D. H. Seo, S. Jeon and K. Kang, *Energy Environ. Sci.*, 2014, **7**, 538-551.
- 182 X. F. Wang, X. H. Lu, Y. X. Tong and G. Z. Shen, *Adv. Mater.*, 2014, **26**, 4763-4782.
- 70 183 S. Xu, Y. H. Zhang, J. Cho, J. Lee, X. Huang, L. Jia, J. A. Fan, Y. W. Su, J. Su, H. G. Zhang, H. Y. Cheng, B. W. Lu, C. J. Yu, C. Chuang, T. I. Kim, T. Song, K. Shigetani, S. Kang, C. Dagdeviren, I. Petrov, P. V. Braun, Y. G. Huang, U. Paik and J. A. Rogers, *Nat. Comm.*, 2013, **4**, 1543(1-28).
- 75 184 P. Simon and Y. Gogotsi, *Nat. Mater.*, 2008, **7**, 845-854.
- 185 Y. P. Zhai, Y. Q. Dou, D. Y. Zhao, P. F. Fulvio, R. T. Mayes and S. Dai, *Adv. Mater.*, 2011, **23**, 4828-4850.
- 186 Y. M. He, W. J. Chen, C. T. Gao, J. Y. Zhou, X. D. Li and E. Q. Xie, *Nanoscale*, 2013, **5**, 8799-8820.
- 80 187 C. Niu, E. K. Sichel, R. Hoch, D. Moy and H. Tennent, *Appl. Phys. Lett.*, 1997, **70**, 1480-1482.
- 188 D. N. Futaba, K. Hata, T. Yamada, T. Hiraoka, Y. Hayamizu, Y. Kakudate, O. Tanaike, H. Hatori, M. Yumura and S. Iijima, *Nat Mater.*, 2006, **5**, 987-994.
- 85 189 Z. Niu, W. Zhou, J. Chen, G. Feng, H. Li, W. Ma, J. Li, H. Dong, Y. Ren, D. Zhao and S. Xie, *Energy Environ. Sci.*, 2011, **4**, 1440-1446.
- 190 C. Zheng, W. Qian, C. Cui, Q. Zhang, Y. Jin, M. Zhao, P. Tan and F. Wei, *Carbon*, 2012, **50**, 5167-5175.
- 90 191 G. Xu, C. Zheng, Q. Zhang, J. Huang, M. Zhao, J. Nie, X. Wang and F. Wei, *Nano Res.*, 2011, **4**, 870-881.
- 192 Q. Guo, X. Zhou, X. Li, S. Chen, A. Seema, A. Greiner and H. Hou, *J. Mater. Chem.*, 2009, **19**, 2810-2816.
- 95 193 Z. Chen, V. Augustyn, X. Jia, Q. Xiao, B. Dunn and Y. Lu, *ACS Nano*, 2012, **6**, 4319-4327.
- 194 X. Zhang, W. Shi, J. Zhu, D. J. Kharistal, W. Zhao, B. S. Lalia, H. H. Hng and Q. Yan, *ACS Nano*, 2011, **5**, 2013-2019.
- 195 Z. Chen, Y. Qin, D. Weng, Q. Xiao, Y. Peng, X. Wang, H. Li, F. Wei and Y. Lu, *Adv. Funct. Mater.*, 2009, **19**, 3420-3426.
- 100 196 Z. Niu, P. Luan, Q. Shao, H. Dong, J. Li, J. Chen, D. Zhao, L. Cai, W. Zhou, X. Chen and S. Xie, *Energy Environ. Sci.*, 2012, **5**, 8726-8733.
- 197 S. D. Perera, B. Patel, N. Nijem, K. Roodenko, O. Seitz, J. P. Ferraris, Y. J. Chabal and K. J. Balkus, *Adv. Energy Mater.*, 2011, **1**, 936-945.
- 105 198 C. Meng, C. Liu, L. Chen, C. Hu and S. Fan, *Nano Lett.*, 2010, **10**, 4025-4031.
- 199 L. Yang, S. Cheng, Y. Ding, X. Zhu, Z. L. Wang and M. Liu, *Nano Lett.*, 2011, **12**, 321-325.
- 110 200 L. Huang, D. Chen, Y. Ding, S. Feng, Z. L. Wang and M. Liu, *Nano Lett.*, 2013, **13**, 3135-3139.
- 201 L. Hu, H. Wu and Y. Cui, *Appl. Phys. Lett.*, 2010, **96**, 183502.
- 202 K. Yu Jin, C. Haegheun, H. Chi-Hwan and K. Woong, *Nanotechnology*, 2012, **23**, 065401.
- 115 203 L. Nyholm, G. Nyström, A. Mihranyan and M. Strømme, *Adv. Mater.*, 2011, **23**, 3751-3769.
- 204 P. Karthika, N. Rajalakshmi and K. S. Dhathathreyan, *ChemPhysChem*, 2013, **14**, 3822-3826.
- 205 S. Ju, J. Li, J. Liu, P.-C. Chen, Y.-g. Ha, F. Ishikawa, H. Chang, C. Zhou, A. Facchetti, D. B. Janes and T. J. Marks, *Nano Lett.*, 2007, **8**, 997-1004.
- 120 206 P.-C. Chen, G. Shen, S. Sukcharoenchoke and C. Zhou, *Appl. Phys. Lett.*, 2009, **94**, 043113.
- 207 J. Ge, G. Cheng and L. Chen, *Nanoscale*, 2011, **3**, 3084-3088.
- 125 208 H. Y. Jung, M. B. Karimi, M. G. Hahm, P. M. Ajayan and Y. J. Jung, *Sci. Rep.*, 2012, **2**.
- 209 K. Wang, H. Wu, Y. Meng, Y. Zhang and Z. Wei, *Energy Environ. Sci.*, 2012, **5**, 8384-8389.
- 210 P.-C. Chen, G. Shen, Y. Shi, H. Chen and C. Zhou, *ACS Nano*, 2010, **4**, 4403-4411.
- 130 211 M. F. El-Kady, V. Strong, S. Dubin and R. B. Kaner, *Science*, 2012, **335**, 1326-1330.
- 212 K. Jost, C. R. Perez, J. K. McDonough, V. Presser, M. Heon, G. Dion and Y. Gogotsi, *Energy Environ. Sci.*, 2011, **4**, 5060-5067.
- 135 213 J. Xu, Q. Wang, X. Wang, Q. Xiang, B. Liang, D. Chen and G. Shen, *ACS Nano*, 2013, **7**, 5453-5462.
- 214 X. Lu, M. Yu, G. Wang, T. Zhai, S. Xie, Y. Ling, Y. Tong and Y. Li, *Adv. Mater.*, 2012, **25**, 267-272.
- 140 215 X. Lu, G. Wang, T. Zhai, M. Yu, S. Xie, Y. Ling, C. Liang, Y. Tong and Y. Li, *Nano Lett.*, 2012, **12**, 5376-5381.

- 216 Q. Wang, J. Xu, X. Wang, B. Liu, X. Hou, G. Yu, P. Wang, D. Chen and G. Shen, *ChemElectroChem*, 2014, **1**, 559-564.
- 217 L. Hu, M. Pasta, F. L. Mantia, L. Cui, S. Jeong, H. D. Deshazer, J. W. Choi, S. M. Han and Y. Cui, *Nano Lett.*, 2010, **10**, 708-714.
- 5 218 M. Pasta, F. La Mantia, L. Hu, H. Deshazer and Y. Cui, *Nano Res.*, 2010, **3**, 452-458.
- 219 J. Xue, Y. Zhao, H. Cheng, C. Hu, Y. Hu, Y. Meng, H. Shao, Z. Zhang and L. Qu, *Phys. Chem. Chem. Phys.*, 2013, **15**, 8042-8045.
- 220 J. Xu, H. Wu, C. Xu, H. Huang, L. Lu, G. Ding, H. Wang, D. Liu, G. Shen, D. Li and X. Chen, *Chem. Eur. J.*, 2013, **19**, 6451-6458.
- 10 221 K. Wang, P. Zhao, X. Zhou, H. Wu and Z. Wei, *J. Mater. Chem.*, 2011, **21**, 16373-16378.
- 222 V. T. Le, H. Kim, A. Ghosh, J. Kim, J. Chang, Q. A. Vu, D. T. Pham, J.-H. Lee, S.-W. Kim and Y. H. Lee, *ACS Nano*, 2013, **7**, 5940-5947.
- 15 223 K. Wang, Q. Meng, Y. Zhang, Z. Wei and M. Miao, *Adv. Mater.*, 2013, **25**, 1494-1498.
- 224 J. Bae, M. K. Song, Y. J. Park, J. M. Kim, M. Liu and Z. L. Wang, *Angew. Chem. Int. Ed.*, 2011, **50**, 1683-1687.
- 225 Z. Yang, J. Deng, X. Chen, J. Ren and H. Peng, *Angew. Chem. Int. Ed.*, 2013, **125**, 13695-13699.
- 20 226 B. Liu, D. Tan, X. Wang, D. Chen and G. Shen, *Small*, 2013, **9**, 1998-2004.
- 227 B. O'Regan and M. Gratzel, *Nature*, 1991, **353**, 737-740.
- 228 J. Burschka, N. Pellet, S.-J. Moon, R. Humphry-Baker, P. Gao, M. K. Nazeeruddin and M. Gratzel, *Nature*, 2013, **499**, 316-319.
- 25 229 M. Gratzel, *Nature*, 2001, **414**, 338-344.
- 230 J. Akilavasan, K. Wijeratne, H. Moutinho, M. Al-Jassim, A. R. M. Alamoud, R. M. G. Rajapakse and J. Bandara, *J. Mater. Chem. A*, 2013, **1**, 5377-5385.
- 30 231 M. Ye, X. Xin, C. Lin and Z. Lin, *Nano Lett.*, 2011, **11**, 3214-3220.
- 232 K. Zhu, N. R. Neale, A. Miedaner and A. J. Frank, *Nano Lett.*, 2006, **7**, 69-74.
- 233 C. Y. Jiang, X. W. Sun, K. W. Tan, G. Q. Lo, A. K. K. Kyaw and D. L. Kwong, *Appl. Phys. Lett.*, 2008, **92**, 143101.
- 35 234 S. Gubbala, V. Chakrapani, V. Kumar and M. K. Sunkara, *Adv. Funct. Mater.*, 2008, **18**, 2411-2418.
- 235 Z. Li, Y. Zhou, C. Bao, G. Xue, J. Zhang, J. Liu, T. Yu and Z. Zou, *Nanoscale*, 2012, **4**, 3490-3494.
- 236 Y. Li, D.-K. Lee, J. Y. Kim, B. Kim, N.-G. Park, K. Kim, J.-H. Shin, I.-S. Choi and M. J. Ko, *Energy Environ. Sci.*, 2012, **5**, 8950-8957.
- 40 237 B.-L. Chen, H. Hu, Q.-D. Tai, N.-G. Zhang, F. Guo, B. Sebo, W. Liu, J.-K. Yuan, J.-B. Wang and X.-Z. Zhao, *Electrochim. Acta*, 2012, **59**, 581-586.
- 238 Y.-Y. Kuo and C.-H. Chien, *Electrochim. Acta*, 2013, **91**, 337-343.
- 45 239 J. Di, Z. Yong, Z. Yao, X. Liu, X. Shen, B. Sun, Z. Zhao, H. He and Q. Li, *Small*, 2013, **9**, 148-155.
- 240 D. Kuang, J. r. m. Brilllet, P. Chen, M. Takata, S. Uchida, H. Miura, K. Sumioka, S. M. Zakeeruddin and M. Grätzel, *ACS Nano*, 2008, **2**, 1113-1116.
- 50 241 J.-Y. Liao, B.-X. Lei, H.-Y. Chen, D.-B. Kuang and C.-Y. Su, *Energy Environ. Sci.*, 2012, **5**, 5750-5757.
- 242 A. Vomiero, V. Galstyan, A. Braga, I. Concina, M. Brisotto, E. Bontempi and G. Sberveglieri, *Energy Environ. Sci.*, 2011, **4**, 3408-3413.
- 55 243 W.-Q. Wu, H.-S. Rao, Y.-F. Xu, Y.-F. Wang, C.-Y. Su and D.-B. Kuang, *Sci. Rep.*, 2013, **3**.
- 244 V. Galstyan, A. Vomiero, I. Concina, A. Braga, M. Brisotto, E. Bontempi, G. Faglia and G. Sberveglieri, *Small*, 2011, **7**, 2437-2442.
- 245 D. Li, P.-C. Chang, C.-J. Chien and J. G. Lu, *Chem. Mater.*, 2010, **22**, 5707-5711.
- 60 246 P. Wang, S. M. Zakeeruddin, J. E. Moser, M. K. Nazeeruddin, T. Sekiguchi and M. Gratzel, *Nat. Mater.*, 2003, **2**, 402-407.
- 247 D.-W. Kim and Y.-K. Sun, *J. Power Sources*, 2001, **102**, 41-45.
- 248 M. G. Kang, K. M. Kim, K. S. Ryu, S. H. Chang, N.-G. Park, J. S. Hong and K.-J. Kim, *J. Electrochem. Soc.*, 2004, **151**, E257-E260.
- 65 249 J.-Y. Park, J.-W. Lee, K. Park, T.-Y. Kim, S.-H. Yim, X. Zhao, H.-B. Gu and E. Jin, *Polym. Bull.*, 2013, **70**, 507-515.
- 250 E. Olsen, G. Hagen and S. Eric Lindquist, *Sol. Energy Mater. Sol. Cells*, 2000, **63**, 267-273.
- 70 251 X. Xu, D. Huang, K. Cao, M. Wang, S. M. Zakeeruddin and M. Grätzel, *Sci. Rep.*, 2013, **3**.
- 252 J. Chen, K. Li, Y. Luo, X. Guo, D. Li, M. Deng, S. Huang and Q. Meng, *Carbon*, 2009, **47**, 2704-2708.
- 253 K.-M. Lee, W.-H. Chiu, H.-Y. Wei, C.-W. Hu, V. Suryanarayanan, W.-F. Hsieh and K.-C. Ho, *Thin Solid Films*, 2010, **518**, 1716-1721.
- 75 254 H. Sun, Y. Luo, Y. Zhang, D. Li, Z. Yu, K. Li and Q. Meng, *J. Phys. Chem. C*, 2010, **114**, 11673-11679.
- 255 M. Wang, A. M. Anghel, B. t. Marsan, N.-L. Cevey Ha, N. Pootrakulchote, S. M. Zakeeruddin and M. Grätzel, *J. Am. Chem. Soc.*, 2009, **131**, 15976-15977.
- 80 256 B. Fan, X. Mei, K. Sun and J. Ouyang, *Appl. Phys. Lett.*, 2008, **93**, 143103.
- 257 J. G. Nam, Y. J. Park, B. S. Kim and J. S. Lee, *Scripta Mater.*, 2010, **62**, 148-150.
- 85 258 K. Suzuki, M. Yamaguchi, M. Kumagai and S. Yanagida, *Chem. Lett.*, 2003, **32**, 28-29.
- 259 F. Malara, M. Manca, L. De Marco, P. Pareo and G. Gigli, *ACS Appl. Mater. Inter.*, 2011, **3**, 3625-3632.
- 260 F. Malara, M. Manca, M. Lanza, C. Hubner, E. Piperopoulos and G. Gigli, *Energy Environ. Sci.*, 2012, **5**, 8377-8383.
- 90 261 L.-Y. Chang, C.-P. Lee, K.-C. Huang, Y.-C. Wang, M.-H. Yeh, J.-J. Lin and K.-C. Ho, *J. Mater. Chem.*, 2012, **22**, 3185-3191.
- 262 K. S. Lee, W. J. Lee, N.-G. Park, S. O. Kim and J. H. Park, *Chem. Commun.*, 2011, **47**, 4264-4266.
- 95 263 C.-W. Kung, H.-W. Chen, C.-Y. Lin, K.-C. Huang, R. Vittal and K.-C. Ho, *ACS Nano*, 2012, **6**, 7016-7025.
- 264 H.-W. Chen, C.-W. Kung, C.-M. Tseng, T.-C. Wei, N. Sakai, S. Morita, M. Ikegami, T. Miyasaka and K.-C. Ho, *J. Mater. Chem. A*, 2013, **1**, 13759-13768.
- 100 265 X. Chen, Y. Hou, B. Zhang, X. H. Yang and H. G. Yang, *Chem. Commun.*, 2013, **49**, 5793-5795.
- 266 T. Chen, L. Qiu, Z. Yang and H. Peng, *Chem. Soc. Rev.*, 2013, **42**, 5031-5041.
- 267 W. Wang, Q. Zhao, H. Li, H. Wu, D. Zou and D. Yu, *Adv. Funct. Mater.*, 2012, **22**, 2775-2782.
- 105 268 J. Velten, Z. Kuanyshbekova, Ö. Göktepe, F. Göktepe and A. Zakhidov, *Appl. Phys. Lett.*, 2013, **102**, 203902.
- 269 L. Chen, Y. Zhou, H. Dai, Z. Li, T. Yu, J. Liu and Z. Zou, *J. Mater. Chem. A*, 2013, **1**, 11790-11794.
- 110 270 S. Hou, X. Cai, H. Wu, Z. Lv, D. Wang, Y. Fu and D. Zou, *J. Power Sources*, 2012, **215**, 164-169.
- 271 W. Guo, C. Xu, X. Wang, S. Wang, C. Pan, C. Lin and Z. L. Wang, *J. Am. Chem. Soc.*, 2012, **134**, 4437-4441.
- 272 Y. Chae, J. T. Park, J. K. Koh, J. H. Kim and E. Kim, *Mater. Sci. Eng., B*, 2013, **178**, 1117-1123.
- 115 273 S. Zhang, C. Ji, Z. Bian, R. Liu, X. Xia, D. Yun, L. Zhang, C. Huang and A. Cao, *Nano Lett.*, 2011, **11**, 3383-3387.
- 274 Z. Lv, J. Yu, H. Wu, J. Shang, D. Wang, S. Hou, Y. Fu, K. Wu and D. Zou, *Nanoscale*, 2012, **4**, 1248-1253.
- 120 275 M. J. Uddin, B. Davies, T. J. Dickens and O. I. Okoli, *Sol. Energy Mater. Sol. Cells*, 2013, **115**, 166-171.
- 276 S. Pan, Z. Yang, P. Chen, X. Fang, G. Guan, Z. Zhang, J. Deng and H. Peng, *J. Phys. Chem. C*, 2013. DOI: 10.1021/jp410402w
- 277 H. Sun, Z. Yang, X. Chen, L. Qiu, X. You, P. Chen and H. Peng, *Angew. Chem.*, 2013, **125**, 8434-8438.
- 125 278 Y. Fu, Z. Lv, S. Hou, H. Wu, D. Wang, C. Zhang, Z. Chu, X. Cai, X. Fan, Z. L. Wang and D. Zou, *Energy Environ. Sci.*, 2011, **4**, 3379-3383.
- 279 B. Weintraub, Y. Wei and Z. L. Wang, *Angew. Chem.*, 2009, **121**, 9143-9147.
- 130 280 T. Chen, L. Qiu, Z. Cai, F. Gong, Z. Yang, Z. Wang and H. Peng, *Nano Lett.*, 2012, **12**, 2568-2572.
- 281 Z. L. Wang and J. H. Song, *Science*, 2006, **312**, 242-246.
- 282 G. Zhu, R. S. Yang, S. H. Wang and Z. L. Wang, *Nano Lett.* 2010, **10**, 3151-3155.
- 135 283 S. Xu, Y. Qin, C. Xu, Y. G. Wei, R. S. Yang and Z. L. Wang, *Nat. Nanotechnol.*, 2010, **5**, 366-373.
- 284 X. F. Wang, B. Liu, R. Liu, Q. F. Wang, X. J. Hou, D. Chen, R. M. Wang and G. Z. Shen, *Angew. Chem. Int. Ed.*, 2014, **53**, 1849-1853.
- 140 285 L. VJ. J.-Y. Oh, A. P. Nayak, A. M. Katzenmeyer, K. H. Cilchrist, S. Grego, N. P. Kobayashi, S.-Y. Wang, A. A. Talin, N. K. Dhar and M. S. Islam, *IEEE J. Sel. Top. Quant. Electron.* 2011, **17**, 1002-1032.

286 D. S. Tsai, W. C. Lien, D. H. Lien, K. M. Chen, M. L. Tsai, D.G. Senesky, Y. C. Yu, A. P. Pisano and J. H. He, *Sci. Rep.*, 2013, **4**.